Enhanced MAPK1 Function Causes a Neurodevelopmental Disorder within the RASopathy Clinical Spectrum

Marialetizia Motta,[1,27] Luca Pannone,[1,2,27] Francesca Pantaleoni,[1] Gianfranco Bocchinfuso,[3] Francesca Clementina Radio,[1] Serena Cecchetti,[4] Andrea Ciolfi,[1] Martina Di Rocco,[2,5] Mariet W. Elting,[6] Eva H. Brilstra,[7] Stefania Boni,[8] Laura Mazzanti,[9] Federica Tamburrino,[9] Larry Walsh,[10] Katelyn Payne,[10] Alberto Fernández-Jaén,[11] Mythily Ganapathi,[12] Wendy K. Chung,[13] Dorothy K. Grange,[14] Ashita Dave-Wala,[15] Shalini C. Reshmi,[15,16] Dennis W. Bartholomew,[15] Danielle Mouhlas,[15] Giovanna Carpentieri,[1,2] Alessandro Bruselles,[2] Simone Pizzi,[1] Emanuele Bellacchio,[1] Francesca Piceci-Sparascio,[17] Christina Lißewski,[18] Julia Brinkmann,[18] Ronald R. Waclaw,[19] Quinten Waisfisz,[6] Koen van Gassen,[7] Ingrid M. Wentzensen,[20] Michelle M. Morrow,[20] Sara Álvarez,[21] Mónica Martínez-García,[21] Alessandro De Luca,[17] Luigi Memo,[22] Giuseppe Zampino,[23] Cesare Rossi,[24] Marco Seri,[24] Bruce D. Gelb,[25] Martin Zenker,[18] Bruno Dallapiccola,[1] Lorenzo Stella,[3] Carlos E. Prada,[19,26] Simone Martinelli,[2,28] Elisabetta Flex,[2,28] and Marco Tartaglia[1,28,*]

Signal transduction through the RAF-MEK-ERK pathway, the first described mitogen-associated protein kinase (MAPK) cascade, mediates multiple cellular processes and participates in early and late developmental programs. Aberrant signaling through this cascade contributes to oncogenesis and underlies the RASopathies, a family of cancer-prone disorders. Here, we report that *de novo* missense variants in *MAPK1*, encoding the mitogen-activated protein kinase 1 (i.e., extracellular signal-regulated protein kinase 2, ERK2), cause a neurodevelopmental disease within the RASopathy phenotypic spectrum, reminiscent of Noonan syndrome in some subjects. Pathogenic variants promote increased phosphorylation of the kinase, which enhances translocation to the nucleus and boosts MAPK signaling *in vitro* and *in vivo*. Two variant classes are identified, one of which directly disrupts binding to MKP3, a dual-specificity protein phosphatase negatively regulating ERK function. Importantly, signal dysregulation driven by pathogenic *MAPK1* variants is stimulus reliant and retains dependence on MEK activity. Our data support a model in which the identified pathogenic variants operate with counteracting effects on MAPK1 function by differentially impacting the ability of the kinase to interact with regulators and substrates, which likely explains the minor role of these variants as driver events contributing to oncogenesis. After nearly 20 years from the discovery of the first gene implicated in Noonan syndrome, *PTPN11*, the last tier of the MAPK cascade joins the group of genes mutated in RASopathies.

Introduction

Signaling through the RAF-MEK-ERK pathway, the first described mitogen-associated protein kinase (MAPK) cascade, mediates multiple cellular processes in response to growth factors, cytokines, and hormones.[1,2] Due to its nodal role in signal transduction, signal traffic through this cascade is tightly controlled, and enhanced flow through it is a well-characterized event contributing to oncogenesis.[3] At the organism level, MAPK signaling participates in early and late developmental programs, including organogenesis, morphology determination, synaptic plasticity, and growth.[4–6] Consistently, germline mutations in genes encoding proteins with a role in the RAS-MAPK signaling cascade or having a functional link to this pathway have been linked causally to the RASopathies, a family of genetic disorders sharing distinctive facial dysmorphisms, short stature, variable cognitive impairment and behavioral problems,

[1]Genetics and Rare Diseases Research Division, Ospedale Pediatrico Bambino Gesù, IRCCS, 00146 Rome, Italy; [2]Department of Oncology and Molecular Medicine, Istituto Superiore di Sanità, 00161 Rome, Italy; [3]Department of Chemical Science and Technologies, University of Rome Tor Vergata, 00133, Rome, Italy; [4]Microscopy Area, Core Facilities, Istituto Superiore di Sanità, 00161 Rome, Italy; [5]Department of Biochemical Science "A. Rossi Fanelli," Sapienza University of Rome, 00185 Rome, Italy; [6]Department of Clinical Genetics, Amsterdam UMC, Vrije Universiteit, 1117 Amsterdam, the Netherlands; [7]Department of Genetics, University Medical Center Utrecht, 3584 CX Utrecht, the Netherlands; [8]Medical Genetics Unit, S. Martino Hospital, 32100 Belluno, Italy; [9]Department of Medical and Surgical Sciences, Policlinico S. Orsola-Malpighi Hospital, University of Bologna, 40138 Bologna, Italy; [10]Indiana University Health at Riley Hospital for Children, Indianapolis, IN 46202, USA; [11]Department of Pediatrics Neurology, Hospital Universitario Quirón de Madrid, Universidad Europea de Madrid, 28223 Madrid, Spain; [12]Department of Pathology and Cell Biology, Columbia University Medical Center, New York, NY 10032, USA; [13]Departments of Pediatrics and Medicine, Columbia University Medical Center, New York, NY 10032, USA; [14]Department of Pediatrics, Division of Genetics and Genomic Medicine, Washington University School of Medicine, St. Louis, MO 63110, USA; [15]Institute for Genomic Medicine, Nationwide Children's Hospital, Columbus, OH 43215, USA; [16]Department of Pediatrics, Nationwide Children's Hospital, Columbus, OH 43215, USA; [17]Medical Genetics Division, Fondazione IRCCS Casa Sollievo della Sofferenza, 71013 San Giovanni Rotondo, Italy; [18]Institute of Human Genetics, University Hospital Magdeburg, 39120 Magdeburg, Germany; [19]Department of Pediatrics, University of Cincinnati College of Medicine, Cincinnati, OH 45229, USA; [20]GeneDx, Gaithersburg, 20877 MD, USA; [21]Medical Department, NimGenetics, 28049 Madrid, Spain; [22]Ambulatorio Genetica Clinica, Ospedale San Bortolo, 36100 Vicenza, Italy; [23]Center for Rare Disease and Congenital Defects, Fondazione Policlinico Universitario Gemelli, Università Cattolica del Sacro Cuore, 00168 Rome, Italy; [24]Medical Genetics Unit, Policlinico S. Orsola-Malpighi, University of Bologna, 40138 Bologna, Italy; [25]Mindich Child Health and Development Institute and Department of Pediatrics, Icahn School of Medicine at Mount Sinai, New York, NY 10029, USA; [26]Division of Human Genetics, Cincinnati Children's Hospital Medical Center, Cincinnati, OH 45229, USA
[27]These authors equally contributed to this work
[28]These authors equally contributed to this work
*Correspondence: marco.tartaglia@opbg.net
https://doi.org/10.1016/j.ajhg.2020.06.018.
© 2020 American Society of Human Genetics.

and a wide spectrum of cardiac defects as major features.[7–9] These syndromes are also characterized by a variably increased risk for certain childhood malignancies, including rhabdomyosarcoma, neuroblastoma, brain tumors, acute leukemias, and juvenile myelomonocytic leukemia.[10–12] Notably, these discoveries have elucidated a paradigm with two major "classes" of activating pathogenic variants involving proteins of the RAS-MAPK pathway, somatic defects in cancer and germline lesions in RASopathies, that have differential impacts on cell transformation and development.[7,13]

Noonan syndrome (NS [MIM: PS163950]), the most common and clinically variable disorder among the RASopathies,[14] is genetically heterogeneous and is caused by pathogenic variants in more than ten genes encoding proteins with roles in the RAS-MAPK signaling cascade or having functional links to this pathway, with variation in *PTPN11* (MIM: 176876),[15] *SOS1* (MIM: 182530),[16,17] *RAF1* (MIM: 164760),[18,19] *RIT1* (MIM: 609591),[20] and *LZTR1* (MIM: 600574)[21,22] accounting for the majority of cases. In about 10%–20% of affected individuals, however, the clinical diagnosis is not molecularly confirmed, suggesting that additional genes are likely implicated in the pathogenesis of this disorder or raising the possibility that other still unrecognized RASopathies (i.e., diseases caused by RAS-MAPK signaling dysregulation) or genocopies (i.e., diseases with significant clinical overlap with NS but caused by distinct molecular mechanisms) may account for these affected individuals.

In this study, we established that *de novo* missense variants in *MAPK1*, encoding the mitogen-activated protein kinase 1 (also known as extracellular signal-regulated protein kinase 2, ERK2), underlie a neurodevelopmental disorder within the clinical spectrum of the RASopathies. We characterized the clinical profile of seven unrelated affected individuals and used primary fibroblasts and cell lines ectopically expressing individual mutant alleles to demonstrate that these mutations promote stimulus-dependent gain-of-function (GoF) of the kinase and enhance MAPK signaling *in vitro*. Knock-in and transgenic *mpk-1* lines in *Caenorhabditis elegans* (*C. elegans*) were used to demonstrate the activating behavior of the tested amino acid substitutions *in vivo*. Our *in silico* and *in vitro* analyses indicate that the identified variants operate with counteracting effects on MAPK1 function by differentially impacting the ability of the kinase to interact with regulators and substrates and that their GoF retains dependence on MEK activity, which likely explains the minor impact of *MAPK1* variation as a driver event in oncogenesis.

Subjects and Methods

Subjects

The study was approved by the local Institutional Ethical Committee of the Ospedale Pediatrico Bambino Gesù, Rome. Subjects 1 and 2 were analyzed in the frame of dedicated research projects focused on RASopathies, while the other individuals were referred for diagnostic genetic testing. Clinical data and DNA specimens were collected, stored, and used following procedures in accordance with the ethical standards of the declaration of Helsinki protocols, with signed informed consents from the participating subjects/families. Explicit permission was obtained to publish the photographs of the subjects as shown in Figure 1.

Exome Sequencing Analyses

Whole-exome sequencing (WES) was performed using DNA samples obtained from leukocytes. A trio-based strategy was used in all cases. Target enrichment kits, sequencing platforms, and WES statistics are reported in Table S1. WES data processing, sequence alignment to GRCh37, and variant filtering and prioritization by allele frequency, predicted functional impact, and inheritance models were performed using the indicated pipeline (UMCUGenetics/IAP; subject 5) or as previously reported.[23–29] WES data output is summarized in Table S2. The *de novo* origin of the *MAPK1* mutations was confirmed by Sanger sequencing in all cases (primer sequences are available on request).

Expression Constructs and Primary Cell Lines

The entire *MAPK1* coding sequence was cloned into the pcDNA6/Xpress-HisA eukaryotic expression vector (*in vitro* studies). Mutations were introduced using primed amplification by polymerase chain reaction (site-directed mutagenesis), as previously described.[30] Constructs were subcloned into the pB255 vector (a gift from S. Takagi, University of Nagoya) (*in vivo* studies). All constructs were Sanger sequenced bidirectionally for their entire open reading frame. Subject 2's primary fibroblasts were obtained from skin biopsy after signed informed consent, following standard procedures. Human Lenti-X 293T, HEK293T, and fibroblast cells were maintained in DMEM medium supplemented with 10% heat-inactivated FBS, 1% L-glutamine, and antibiotics.

In Vitro Studies

Transient transfections and MAPK/RSK/MCL1 phosphorylation assays were performed as previously reported.[24,31,32]

Experiments used the following antibodies: mouse monoclonal anti-Xpress (Invitrogen); mouse monoclonal anti-Myc, rabbit polyclonal anti-p44/42 MAPK1/3 (ERK2/1), mouse monoclonal anti-phospho-p44/42 MAPK1/3 (ERK2/1) (Thr202/Tyr204 of Erk1 and Thr185 and Tyr187 of Erk2), rabbit polyclonal anti-MCL1, rabbit polyclonal anti-phospho-MCL1 (Ser159/Thr163), rabbit monoclonal anti-RSK1/RSK2/RSK3 (32D7), rabbit polyclonal anti-phospho-p90RSK (Thr359/Ser363) (Cell Signaling Technology); mouse monoclonal anti-MKP3 and mouse monoclonal anti-GAPDH (Santa Cruz); horseradish peroxidase-conjugated anti-rabbit or anti-mouse (Sigma-Aldrich).

MAPK/RSK/MCL1 phosphorylation assays after treatment with trametinib were performed on transfected HEK293T cells seeded in 6-well plates the day before transfection (70% to 80% confluence) and on subconfluent primary fibroblasts. Cells were serum starved for 16 h and then treated with the MEK1 inhibitor (1.5 ng/mL, 2 h) or left untreated, and then stimulated with EGF (transfected cells: 30 ng/mL, 1 min; primary fibroblasts: 10 ng/mL, 15 min) or left unstimulated.

MAPK1/MEK1 co-IP assays were performed on serum-starved transfected HEK293T cells, while MAPK1/MKP3 co-IP experiments were performed on transfected HEK293T cells and primary fibroblasts serum starved for 16 h, and then stimulated with EGF (transfected cells: 30 ng/mL, 1 min; primary fibroblasts: 10 ng/mL, 15 min), as reported.[33]

Figure 1. Clinical Features of Individuals with *De Novo MAPK1* Variants
Facial features of subjects 1 to 7. Note the occurrence of hypertelorism, downslanting palpebral fissures, ptosis, low-set/posteriorly rotated ears with evident antitragus and earlobes with central depression, long philtrum with evident columns, marked upper lip vermilion and everted lower lip, and short/webbed neck. Craniofacial features resemble NS or a related RASopathy in subjects 1, 2, 3, 4, and 6. The evolving phenotype of subject 2 with age is reported in Figure S3.

Transactivation reporter assays were performed using Lenti-X 293T cells seeded in 12-well plates the day before transfection. Monolayers were transfected with the following plasmids: pFR-Luc (a reporter plasmid in which luciferase expression is driven by minimal promoters for ELK1), pFA2-Elk1, pRL-TK-Renilla, and vectors expressing wild-type MAPK1 or each of the tested mutants. At 24 h after transfection, cells were serum starved for 18 h and then stimulated with EGF (30 ng/mL) for 5 h or left unstimulated. Normalized luciferase levels were reported as fold activation over vector expressing MAPK1, basally.

For nuclear translocation analyses, Lenti-X 293T cells were seeded at the density of 3×10^3 in 24-well cluster plates onto 12 mm cover glasses. After 24 h of culture in complete medium, cells were transfected with the pcDNA6 constructs. At 24 h after transfection, cells were serum starved for 18 h and then treated with EGF (30 ng/mL, 5 min) or left unstimulated and fixed with 3% paraformaldehyde. Fixed cells were permeabilized with 0.5% Triton X-100 and stained with a mouse monoclonal anti-Xpress followed by goat anti-mouse Alexa Fluor 594 and then with phalloidin antibody conjugated to green-fluorescent Alexa Fluor 488 dye (Invitrogen). After staining, coverslips were extensively rinsed and then mounted on the microscope slide by using Vectashield with DAPI mounting medium (Vector Laboratories). Confocal analysis was performed on a Zeiss LSM 980 with Airyscan2, using the 63× oil objective and excitation spectral laser lines at 405 and 488 nm. Cells stained only with the fluorochrome-conjugated secondary antibodies were used to set up acquisition parameters. Signals from different fluorescent probes were taken in sequential scanning mode.

C. elegans Studies

Culture, maintenance, germline transformation, and genetic crosses were performed using standard techniques.[34,35] The Bristol N2 (wild-type animals) and PS21 (*let-23*(*sy1*) II; *him-5*(*e1490*) V) strains were provided by the *Caenorhabditis Genetics Center* (CGC,

University of Minnesota, Minneapolis, MN). *let-23*(*sy1*) is a hypomorphic allele of *let-23* (ortholog of the human *EGFR* gene) harboring a nonsense mutation leading to the lack of the last six amino acids and originally isolated as suppressor of the multivulva phenotype of *lin-15*(*n309*) animals.[36,37] The engineered change to the endogenous *mpk-1 locus* was carried out by CRISPR-Cas9 as previously described.[38] A total of 20 wild-type animals were injected with a mix containing 750 ng/μL Cas9 (IDT), 700 ng/μL ALT-R CRISPR tracrRNA (IDT), 115 ng/μL *dpy-10* crRNA (5′-CTCGTGGTGCCTATGGTAGC-3′), 37.5 ng/μL ssODN *dpy-10* (5′-ATAGGCTGTTGGTCTGAAGCCATGTGAAGCTCCGCTACCATAG GCACCGCATGCGGTACGGTTTCCAGTCATTCTCATCTTGCCGT ATTGAAGTTCAAGTG-3′), 350 ng/μL *mpk-1* crRNA (5′-TCACAA ACTGGCTCATCTCC-3′), and 175 ng/μL ssODN *mpk-1*[D321G] (5′-ATTTCGATTTTCAGTATCGACATCGAGCAAGCATTAGCACAT CCTTATTTAGAACAGTATTATGGTCCTGGTGATGAGCCAGTTT GTGAGGAACCATTCACTTTGGA-3′). Worms were then recovered on normal growth medium (NGM) at 20°C. Animals with a roller (rol) or a dumpy (dpy) phenotype were isolated, as well as pools of five wild-type hermaphrodites from jackpot plates (i.e., plates with several rol and dpy animals). To isolate worms harboring the *mpk-1* variant, PCR amplification was performed using a single forward primer (5′-GGCTGTGTCGATTTACGTACG-3′) and two reverse primers annealing with the wild-type (5′-GGTGCATTCACATCA-CAGCTG-3′) or the modified (5′-GCACACAGGTTCGTCAC-CAGG-3′) sequence. Homozygosity was confirmed by Sanger sequencing. Three independent lines harboring the desired change were generated; two of them were backcrossed three times to the N2 strain to remove any potential off-target mutation and were used for further analyses and crosses. These lines showed an equivalent phenotype and were designated as *mpk-1*(*pan14* [D321G]).

The wild-type *MAPK1* cDNA and a subset of mutant alleles were subcloned into the pB255 vector to be under the control of the *lin-31* promoter (p*lin-31*) and were injected at 100 ng/μL to generate multi-copy extrachromosomal arrays. The pJM371 plasmid (p*elt-2*::*NLS*::*GFP*) (a gift from J.D. McGhee, University of Calgary), driving GFP expression in intestinal cell nuclei, was used as co-injection marker (30 ng/μL). Phenotypic analysis was performed on three independent lines for each construct.

L3/L4 larvae and adult hermaphrodites were scored quantitatively for assessing vulval induction (larvae) and for the presence of multiple ectopic pseudovulvae (multivulva, Muv phenotype) and lack of a vulva (vulvaless, Vul phenotype) (adults). Muv and Vul were scored at a Leica MZ10F dissecting microscope, while vulval induction was evaluated using an Eclipse Ti2-E microscope (Nikon) equipped with DIC optics on live animals mounted on 2% agarose pads containing 10 mM sodium azide as anesthetic. *let-23*(*sy1*) hermaphrodites are egg-laying defective (Egl phenotype) due to the lack of a functional vulva, and larvae accumulate and hatch inside the mother resulting in a bag-of-worms phenotype (Bag). Based on that, the prevalence of Vul in *let-23*(*sy1*);*mpk-1*(D321G) and *let-23*(*sy1*);p*lin-31*::*MAPK1* double mutants was scored blindly at a dissecting microscope by counting the number of eggs retained in the uterus and identifying animals that had become Bag. More specifically, to assess the Egl phenotype, L4 larvae were picked and visually scored after 24 h at 20°C for the accumulation of eggs inside their body, while Bags were later identified by scoring the presence of larvae inside the mother. After each cross, the genotype of individual alleles (*mpk-1* and *let-23*) was confirmed by direct sequencing of the appropriate genomic region. In transgenic experiments, isogenic animals that had lost the transgene were cloned separately and used as controls. p values were calculated using two-tailed Fisher's exact test.

Structural Analyses

Analyses were performed using the UCSF Chimera package.[39] Side chains not solved in the X-ray structures were modeled according to Shapovalov and Dunbrack.[40]

Results

De Novo Missense Variants in *MAPK1* Cause a Neurodevelopmental Disorder within the RASopathy Clinical Spectrum

We performed WES to identify the molecular causes underlying a group of clinically heterogeneous phenotypes with features suggestive of NS or overlapping related RASopathies but without pathogenic variant(s) in previously identified genes. WES data analysis excluded the occurrence of other functionally relevant variants compatible with known Mendelian disorders based on the expected inheritance model and clinical presentation; however, *de novo* missense changes in *MAPK1* were observed in two individuals (c.521C>T [p.Ala174Val], subject 1; c.953A>G [p.Asp318Gly], subject 2; GenBank: NM_002745.4) (Tables S1 and S2). In subject 2, the missense change was confirmed in skin fibroblasts, providing evidence for its germline or early post-zygotic origin. Both variants affected highly conserved residues among MAPK1 orthologs and paralogs (Figure S1), had high CADD scores, and had not previously been reported in gnomAD (Table 1). *MAPK1* is highly intolerant to loss-of-function (LoF) variants (pLI 1.0) and highly constrained for missense variation ($Z = 3.61$),[41] further supporting the clinical relevance of this finding. Networking and connection via GeneMatcher[42] allowed us to identify five additional unrelated subjects carrying a *de novo* missense *MAPK1* substitution (Table 1). In all subjects, no other clinically associated variant was identified (Tables S1 and S2). All *MAPK1* variants were private and affected invariant residues among MAPK1 orthologs and paralogs (Figure S1), and multiple *in silico* prediction algorithms rated these changes as deleterious or pathogenic (Table 1 and Figure S2). Notably, a subset of the identified variants mapped to the cancer-associated *MAPK1* mutation cluster involving Asp321 and Glu322 (COSMIC database). One substitution (c.952G>A [p.Asp318Asn]) affected the same codon as subject 2 (c.953A>G [p.Asp318Gly]), further documenting the non-random distribution of the identified variants. In all samples, no evidence of allelic imbalance was observed (reference versus variant allele ratio between 0.46 and 0.60), strongly suggesting a germline origin of the identified *de novo* variants.

The seven subjects with *de novo MAPK1* mutations shared a neurodevelopmental disorder, with a phenotype reminiscent of RASopathy in a subset of cases (Figures 1 and S3, Table S3). A clinical history of each individual can be found in the Supplemental Note (Case Reports). While the overall phenotype of these subjects appeared

Table 1. List of the Identified Pathogenic *MAPK1* Missense Variants

Nucleotide Change	Amino Acid Change	Domain	Mutation Class	Subject	Origin	REVEL[a]	CADD phred[a]	Metadome d_N/d_S[b]	ACMG[c]
c.221T>A	p.Ile74Asn	active site	2	7	*de novo*	0.82	29.0	0.21	pathogenic
c.238C>T	p.His80Tyr	DRS	1	3	*de novo*	0.88	30.0	0.27	pathogenic
c.521C>T	p.Ala174Val	activation lip	2	1	*de novo*	0.45	23.9	0.10	pathogenic
c.952G>A	p.Asp318Asn	DRS	1	4	*de novo*	0.31	28.9	0.27	pathogenic
c.953A>G	p.Asp318Gly	DRS	1	2	*de novo*	0.39	25.7		pathogenic
c.964G>C	p.Glu322Gln	DRS	1	6	*de novo*	0.31	26.7	0.19	pathogenic
c.968C>G	p.Pro323Arg	DRS	1	5	*de novo*	0.73	28.2	0.18	pathogenic

Nucleotide numbering reflects cDNA numbering with 1 corresponding to the A of the ATG translation initiation codon in the *MAPK1* reference sequence (GenBank: NM_002745.4). No variants were reported in the public databases ExAC and gnomAD.
[a]All variants were predicted to be "deleterious" by Rare Exome Variant Ensemble Learner (REVEL) and/or Combined Annotation Dependent Depletion (CADD) v.1.3 algorithms.[43,44] Scores > 15 (CADDphred) or > 0.5 (REVEL) predict that the sequence change has a significant impact on protein structure and function.
[b]d_N/d_S metric detects evolutionary pressure in protein-coding regions and genomes and is used to measure genetic tolerance.[45] Residues with d_N/d_S values < 0.53 are considered to map within regions "intolerant" to nonsynonymous variation, those with a ratio < 0.18 are supposed to be within "highly intolerant" regions (see Figure S2).
[c]All changes satisfied the necessary criteria to be classified as pathogenic according to the American College of Medical Genetics criteria (see InterVar in Web Resources).[46] c.221T>A: PS2, PS3, PM1, PM2, PP2, PP3. c.238C>T: PS2, PS3, PM1, PM2, PP2, PP3. c.521C>T: PS2, PS3, PM1, PM2, PP2, PP3. c.952G>A: PS2, PS3, PM1, PM2, PP2, PP3. c.953A>G: PS2, PS3, PM1, PM2, PP2, PP3. c.964G>C: PS2, PS3, PM1, PM2, PM5, PP2, PP3. c.968C>G: PS2, PS3, PM1, PM2, PP2, PP3.

variable in terms of severity, it consistently included developmental delay (DD), intellectual disability (ID), and behavioral problems (e.g., ADHD, anxiety, reduced stress tolerance, aggressive behavior). Postnatally reduced growth was documented in approximately half of affected individuals. Craniofacial anomalies were also common, including hypertelorism (5/7 cases), ptosis (6/7 cases), downslanting palpebral fissures (3/7 cases), low-set/posteriorly rotated ears (6/7 cases), wide nasal bridge (3/7cases), and dental anomalies (4/7 cases), which are observed as major recurrent features in RASopathies. Notably, most subjects shared a distinctive ear morphology with evident antitragus and earlobes with central depression, and a long and deep philtrum, marked upper lip vermilion, and everted lower lip. The craniofacial appearance and the co-occurrence of a short/webbed neck, low posterior hairline, skin features (e.g., multiple lentigines, *cafè au lait* spots), and reduced growth substantiated a clinical suspicion of NS or a clinically related trait in subjects 1, 2, 3, 4, and 6. The severe phenotype and peculiar facies of subject 6 was suggestive of cardiofaciocutaneous syndrome (MIM: PS115150). Congenital heart defects, consisting of atrial septal defects and mitral valve insufficiency, were reported in four subjects, but none had cardiomyopathy. Hypotonia and EEG anomalies unmasking potential seizure activity were also noted, which was well controlled by pharmacological treatment (subjects 5 and 6). Minor skeletal defects were also a common finding. Bleeding diathesis and lymphedema occurred in single individuals. None of the subjects was diagnosed with cancer.

MAPK1 Missense Variants Are GoF Alleles

MAPK1 is a ubiquitously expressed protein serine/threonine kinase functioning as terminal tier of the RAS-RAF-MEK-ERK signaling cascade. Its activity requires MEK-mediated phosphorylation of two regulatory phosphorylatable residues, Thr185 and Tyr187, that are located within an activation segment, which favors a conformation of the catalytic domain stabilizing the active site (i.e., DFG-aspartate-in conformation).[16] Dephosphorylation of Thr185 and Tyr187 is catalyzed by MAPK phosphatases (MKPs) and is a required step for the inactivation of the kinase.[47] The reversible phosphorylated state of the two residues controls the magnitude and duration of activation as well as the nuclear localization of the kinase, which, in turn, determine the nature of the cellular response to stimuli. Due to the clinical overlap of some subjects heterozygous for mutant *MAPK1* alleles with NS and the consideration that the latter is caused by upregulated MAPK signaling, we hypothesized a GoF effect of the identified mutations on MAPK1 function. To validate this hypothesis, we assessed the consequences of the disease-associated amino acid substitutions on two key events of MAPK1 function, i.e., its phosphorylation status and translocation to the nucleus. We analyzed the levels of MAPK1 phosphorylation in HEK293T cells transiently transfected with Xpress-tagged *MAPK1* constructs encoding each of the p.Ile74Asn, p.His80Tyr, p.Ala174Val, p.Asp318Gly, p.Asp318Asn, and p.Pro323Arg substitutions, under basal conditions and following EGF stimulation, in time-course experiments (Figure 2A). Ectopic expression of all mutants promoted variably boosted stimulus-dependent MAPK1 phosphorylation, compared to cells overexpressing the wild-type protein, suggesting an activating role of each disease-associated variant. The enhanced stimulus-dependent MAPK1 phosphorylation was confirmed in primary skin fibroblasts from subject 2 (Figure S4, left panel). While MAPK1 is located in the cytoplasm basally, the kinase translocates to the nucleus following stimulation, an event that is required to control the function of a wide variety of transcription factors, chromatin modifying enzymes, and structural proteins modulating gene expression.[48] MAPK1 nuclear translocation is promoted by phosphorylation of the regulatory Thr185 and Tyr187

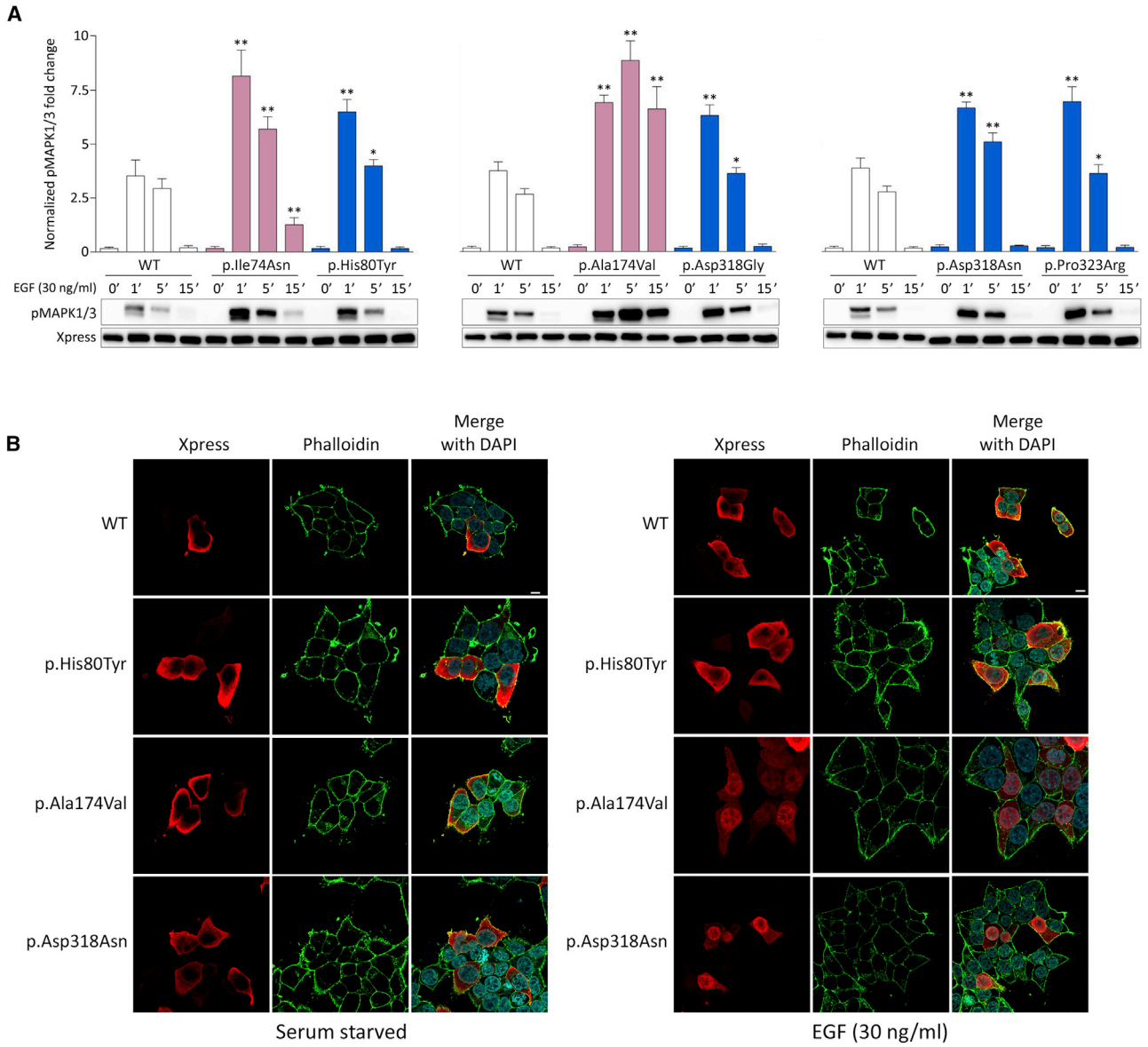

Figure 2. Ectopic Expression of Disease-Causing *MAPK1* Mutant Alleles Promotes a Variably Boosted Stimulus-Dependent Phosphorylation and Nuclear Translocation of MAPK1

(A) MAPK phosphorylation assays. Representative blots (below) and graphs reporting mean ± SD densitometry values (above) of three independent experiments are shown. Affected residues mapping at the DRS are shown in blue, while those mapping at the activation segment are colored in pink. HEK293T cells were transiently transfected with the indicated Xpress-tagged *MAPK1* construct, serum starved (16 h), and stimulated with EGF (30 ng/mL) in time-course experiments or left untreated. Equal amounts of cell lysates were resolved on 10% polyacrylamide gels. Asterisks indicate statistically significant differences in the phosphorylation levels compared to cells overexpressing wild-type MAPK1 at the corresponding experimental points (*$p < 0.05$, **$p < 0.01$; Student's t test).

(B) MAPK1 subcellular localization showed by confocal laser scanning microscopy (CLSM) observations. Panels represent central sections. Assays were performed in Lenti-X 293T cells transiently expressing Xpress-tagged wild-type and three representative MAPK1 mutants, basally (left) and after 5 min of EGF stimulation (right). Similarly to the wild type protein, all mutants localized in the cytoplasm basally, whereas they showed a variably more efficient nuclear translocation after EGF stimulation. Fixed cells were stained with an anti-Xpress mouse monoclonal antibody followed by goat anti-mouse Alexa Fluor-594 (red) and an anti-phalloidin antibody conjugated to green-fluorescent Alexa Fluor 488 dye (green). Nuclei are visualized by DAPI staining (blue). Scale bar is 10 μm. Images referred to the complete set of mutants are reported in Figure S5.

residues, which induces a conformational change allowing the release of the kinase from cytoplasmic anchoring proteins, and its nuclear import via importin-mediated transport.[49] Confocal laser scanning microscopy analysis was performed in Lenti-X 293T cells transiently expressing Xpress-tagged wild-type and mutant *MAPK1* constructs under starved condition and following EGF stimulation. Like the wild-type protein, all disease-associated MAPK1 proteins localized in the cytoplasm basally; however, consistent with their stronger activation following stimulation, they showed a variably more efficient nuclear translocation after treatment with EGF, with amino acid

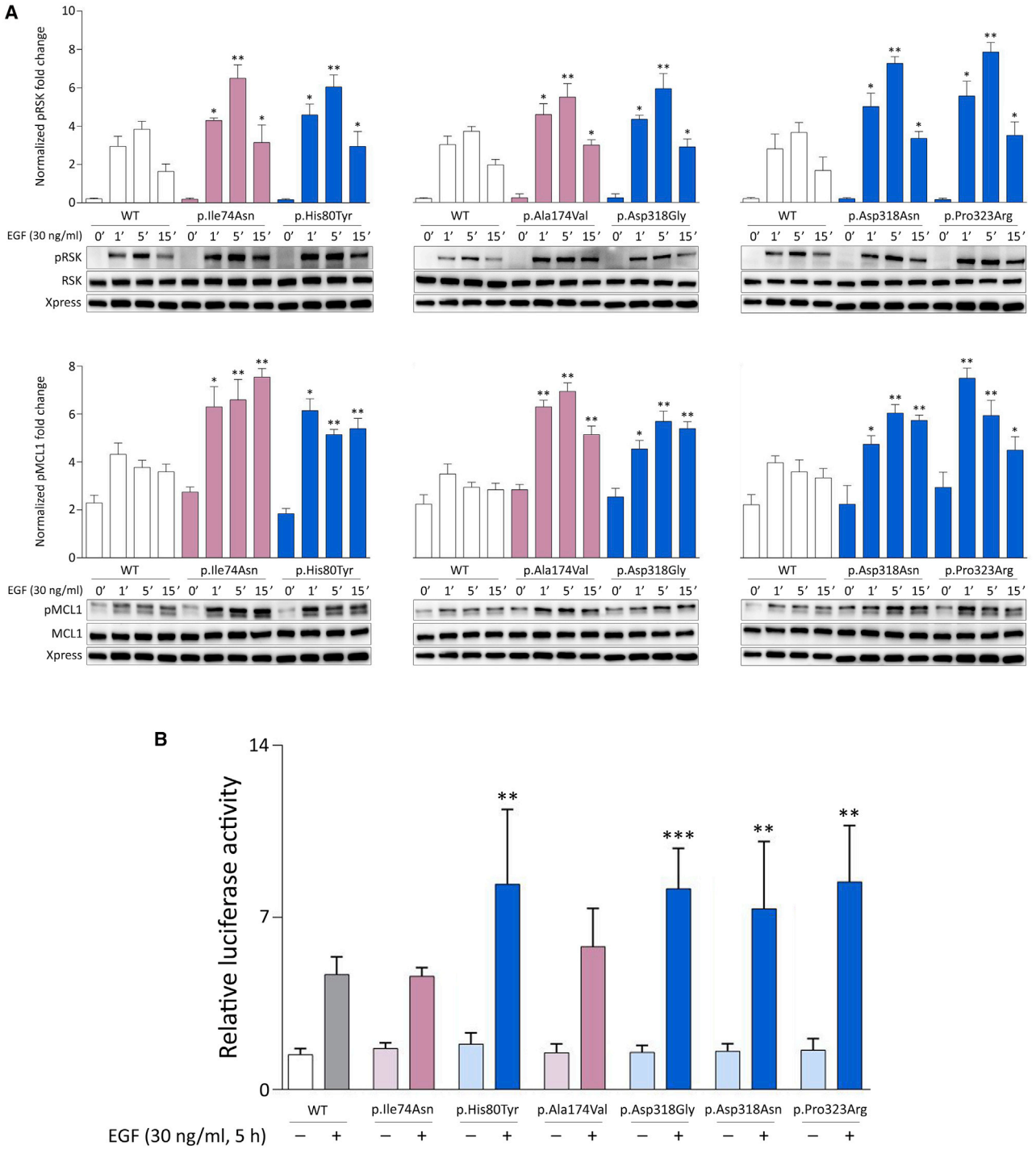

Figure 3. Disease-Causing *MAPK1* Mutations Promote a Variably Enhanced Stimulus-Dependent Activation of the MAPK Signaling Cascade

(A) Overexpression of MAPK1 mutants promote enhanced phosphorylation of RSKs and MCL1, two cytoplasmic substrates of the kinase, as assessed by time-course experiments. Representative blots (below) and graphs reporting mean ± SD densitometry values (above) of three independent experiments are shown. Affected residues mapping at the DRS are shown in blue, while those mapping at the activation segment are colored in pink. HEK293T cells were transiently transfected with the indicated Xpress-tagged *MAPK1* construct, serum starved (16 h), and treated with EGF (30 ng/mL) in time-course experiments or left unstimulated. Equal amounts of cell lysates were resolved on 10% polyacrylamide gels. Asterisks indicate statistically significant differences in the phosphorylation levels compared to cells overexpressing wild-type MAPK1 at the corresponding experimental points (*$p < 0.05$, **$p < 0.01$; Student's t test).

(B) Luciferase assay in Lenti-X 293T cells. Variably enhanced induction of the reporter after EGF stimulation was observed in cells expressing MAPK1 mutants, whereas no difference in the transactivation activity was documented in the unstimulated state. Elk1-induced expression of luciferase was estimated by measuring luciferase activity in lysates prepared from Lenti-X 293T cells cotransfected with

(legend continued on next page)

substitutions at residues Ala174, Asp318, and Pro323 displaying the most robust response (Figures 2B and S5).

To further confirm the GoF role of the identified variants on protein function, we assessed the consequences of ectopic expression of MAPK1 mutants on the phosphorylation status of two well-known cytoplasmic substrates of the kinase, the p90 ribosomal S6 kinases 1-3 (RSK1 to 3) and BCL2-related pro-survival myeloid cell leukemia 1 (MCL1) protein. Immunoblotting analysis showed that the increased MAPK1 phosphorylation associated with overexpression of each mutant resulted in an enhanced phosphorylation of RSKs and MCL1 (Figure 3A), indicating MAPK signaling upregulation. The enhanced RSK phosphorylation was also confirmed in primary fibroblasts from subject 2 (Figure S4, right panel). To specifically assess the function of individual mutants on nuclear substrates, an ELK1 transactivation assay was performed (Figure 3B). When phosphorylated by MAPK1, ELK1 binds to serum responsive elements of promoters to initiate transcription of target genes.[50,51] Lenti-X 293T cells were transfected to co-express either wild-type MAPK1 or each of the six mutants with the *C*-terminal ERK responsive domain of ELK1 fused to the DNA-binding domain of Gal4, a reporter (i.e., luciferase) under the control of a synthetic promoter with five tandemly arranged GAL4 binding sites, and an internal transfection control (i.e., Renilla luciferase). A variably enhanced induction of the reporter after EGF stimulation was observed in cells expressing most mutants, whereas no difference in the transactivation activity was documented in the unstimulated state. Of note, one mutant (p.Ala174Val) was found to have just a slightly increased transactivation activity, while the activity of the p.Ile74Asn mutant was similar to that of the wild-type protein, suggesting a differential impact of mutations involving the activation segment or regions interacting with it on specific functions of the kinase (see below).

In Vivo Assessment of *MAPK1* Variants

To explore the functional impact of the disease-associated *MAPK1* alleles on RAS-MAPK signaling *in vivo*, we used *C. elegans* as a model system. The *mpk-1*/*sur-1* gene, ortholog of *MAPK1*, displays 81% sequence identity and 88% conservation with the human protein (Figure S1). MPK-1 is involved in several LET-60 (RAS)-mediated developmental processes, including vulval cell fate specification.[52] Specifically, LET-60 acts via the canonical MAPK cascade (i.e., LIN-45/RAF, MEK-2/MEK, and MPK-1) to promote hermaphrodite vulval development in cooperation with the WNT and LIN-12 (NOTCH) signaling pathways.[53] Enhanced LET-60 signaling leads to the formation of multiple ectopic pseudovulvae along the ventral side of the animal as a result of hyperinduction of the six vulval precursor cells (VPCs) (multivulva, Muv phenotype). Conversely, when signal flow through LET-60 is turned off, as in the case of defective upstream signaling elicited by the LET-23 (EGFR) tyrosine kinase receptor, VPCs adopt an alternative cell fate resulting in the absence of any vulval tissue (vulvaless, Vul phenotype). In line with the positive role of MPK-1 in LET-60 signaling, LoF *mpk-1* mutations cause a highly penetrant Vul phenotype and suppress the Muv phenotype associated with hyperactive LET-60, while transgenic animals co-expressing GoF mutations of *mpk-1* and *mek-2* alleles under control of the *lin-31* promoter exhibit a high penetrant Muv phenotype.[54–56] Here, we introduced the c.953A>G (p.Asp318Gly) change at the orthologous position of the *C. elegans* gene by CRISPR-Cas9 to generate *mpk-1*(*pan14*[D321G]) knock-in animals (Figure 4A). The resulting nematodes did not show any Vul phenotype, ruling out a LoF/dominant-negative role of the mutation. Conversely, the mutant worms displayed a low penetrant Muv phenotype and partially rescued the Vul phenotype of animals harboring the hypomorphic *let-23* (*sy1*) allele (Figures 4B–4D and Table S4), indicating upregulation of signaling through LET-60 and the MAPK cascade. In line with this evidence, hyperinduction of VPCs was also noted (Figure 4E).

To confirm the GoF behavior of the p.Asp318Gly substitution and extend *in vivo* our analysis to a larger panel of mutants, transgenic lines overexpressing wild-type *MAPK1* or a subset of mutant alleles (those encoding p.Ile74Asn, p.His80Tyr, p.Ala174Val, p.Asp318Gly, and p.Pro323Arg) under the control of p*lin-31*, which drives expression principally in VPCs, were generated and assessed phenotypically. Ectopic expression of the wild-type protein did not elicit any Muv phenotype but slightly ameliorated the Vul phenotype of *let-23*(*sy1*) animals (Table S4), indicating that human MAPK1 works appropriately in the context of the *C. elegans* vulva. Of note, worms overexpressing each of the mutants displayed Muv, although at a low prevalence, and more efficiently rescued the Vul phenotype, with p.Asp318Gly and p.Pro323Arg being the most activating substitutions (Figures 4B and 4C).

Defective Negative MKP3 Regulation Is a Generalizable Mechanism for the GoF Behavior of *MAPK1* Variants

To understand the molecular mechanism(s) by which the identified pathogenic variants promote enhanced MAPK1 function, analysis of the available crystallographic structures of the kinase complexed with regulators and effectors was performed. MAPK1 is characterized by a single kinase domain (residues 25–313), comprising two lobes.[57] The small N-terminal lobe is constituted by a five-stranded antiparallel β sheet (1–5) containing residues involved in

pFR-Luc, pFA2-Elk1, pRL-TK-Renilla, and vectors expressing the wild-type or each of the six MAPK1 mutants. Each value represents luciferase activity in relative light units, which was normalized for Renilla luciferase activity. Three independent experiments were performed, each including duplicate samples. Bars indicate means ± SD. One-way ANOVA ($p = 0.0001$, R square = 0.8913) followed by Bonferroni's multiple comparison test (**$p < 0.005$, ***$p < 0.001$).

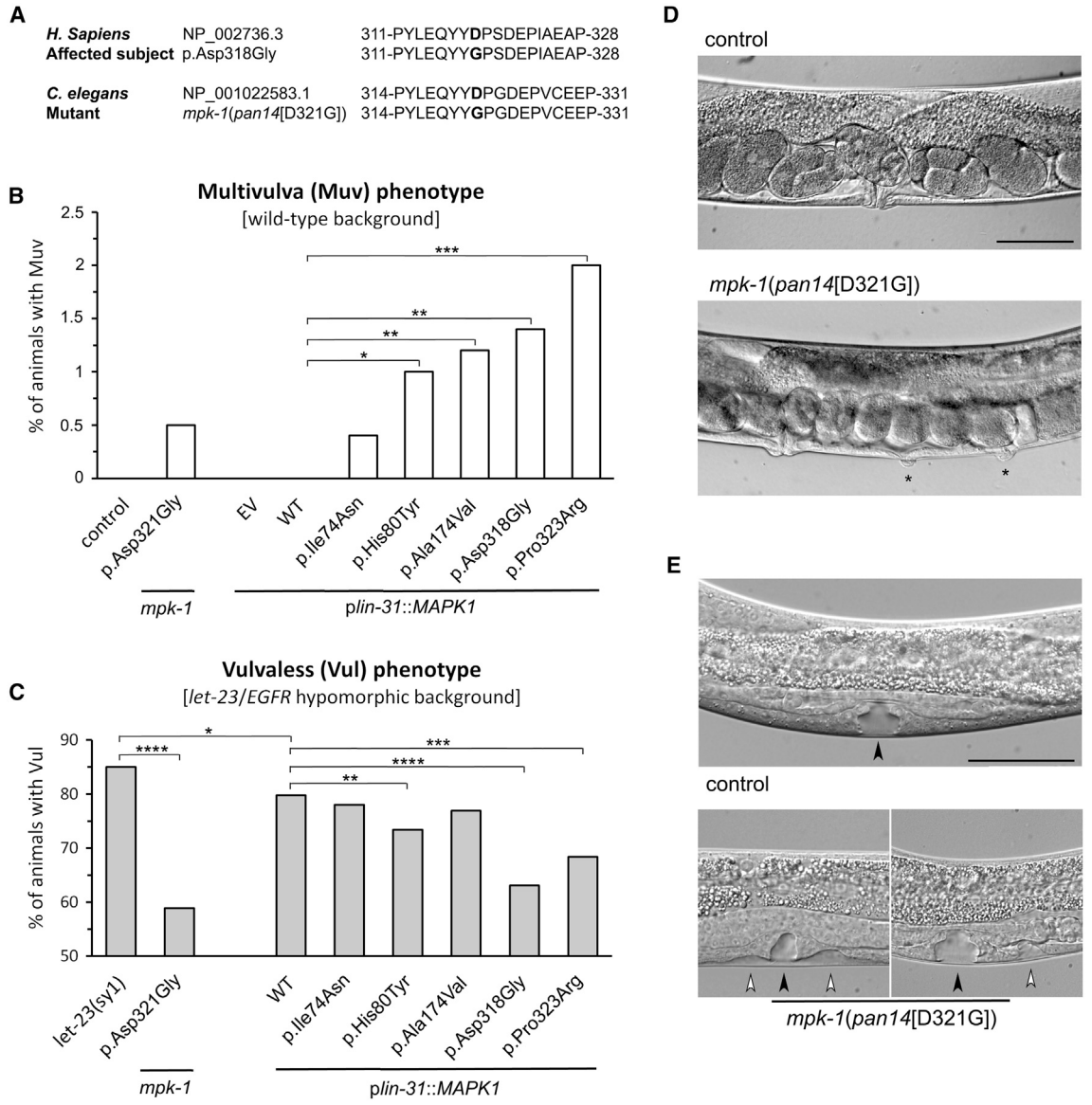

Figure 4. Consequences of *MAPK1* Disease-Causing Variants on *C. elegans* Vulval Development

(A) Amino acid sequences of wild-type and p.Asp318Gly MAPK1, wild-type MPK-1 (ortholog of MAPK1), and *mpk-1*(*pan14*[D321G]) mutant engineered by CRISPR-Cas9. The modified residues are highlighted in bold.

(B) *mpk-1*(*pan14*[D321G]) (p.Asp321Gly) knock-in animals displayed a low penetrant multivulva (Muv) phenotype. A variable prevalence of Muv was also observed in worms overexpressing a subset of disease-causing *MAPK1* alleles under the control of p*lin-31*, which drives expression principally in vulval precursor cells (VPCs). Asterisks specify significant differences from animals expressing $MAPK1^{WT}$ (*$p < 0.02$, **$p < 0.01$, ***$p < 0.0005$; two-tailed Fisher's exact test).

(C) Expression of the mutant alleles ameliorates the vulvaless (Vul) phenotype of animals carrying the hypomorphic *let-23* (*EGFR*) *sy1* allele. Asterisks specify significant differences from *let-23(sy1)* animals (*$p < 0.05$, ****$p < 0.00002$) or from *let-23(sy1)* animals expressing $MAPK1^{WT}$ (**$p < 0.02$, ***$p < 0.002$, ****$p < 0.00002$).

(D) Nomarski images show that a normal vulva develops in control adult hermaphrodites (above), whereas a number of multiple ectopic pseudovulvae are observed in *mpk-1*(*pan14*[D321G]) animals (below). Asterisks indicate the ectopic pseudovulvae.

(E) Nomarski images of vulval precursor cells (VPCs) at late L3/early L4 larval stages. In control animals, only P6.p detaches from the cuticle generating a single, symmetric invagination (above). This process is altered in a minority of L3/L4 larvae carrying the *mpk-1*(*pan14*[D321G]) allele, which show multiple, asymmetric invaginations (below). This phenotype represents the prodromal sign of Muv. Black and white arrowheads point to normal and extra invaginations, respectively. Anterior is to the left and dorsal is up, in all images. Scale bars, 50 μm. EV, empty vector. Number of animals scored are reported in Table S4.

catalysis, an α helix (helix C) that assumes slightly different orientations in the active and inactive states, and a glycine-rich loop, interacting with the ATP phosphates. The large C-terminal lobe comprises six conserved segments and four short conserved β strands containing most of the catalytic residues. The activation segment, close to the active site, represents the most important regulatory element and encompasses the activation lip, where

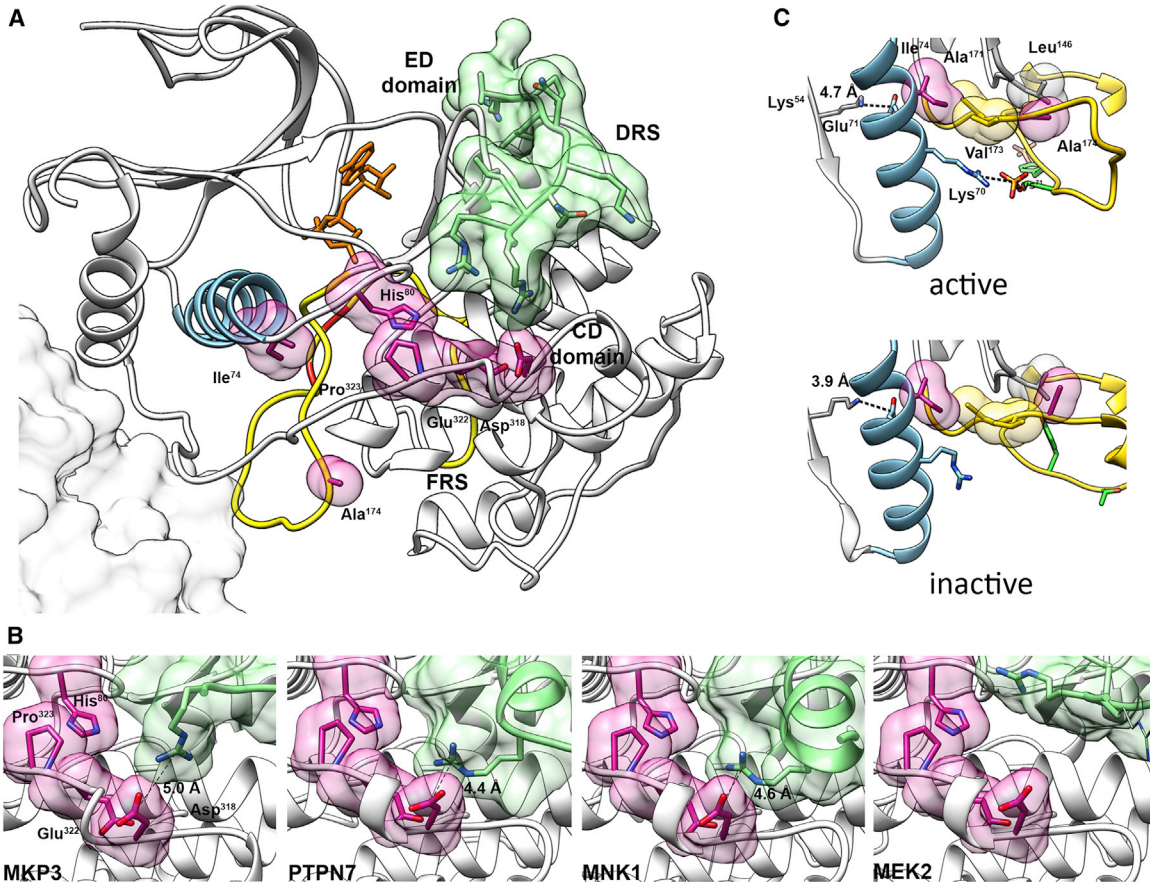

Figure 5. Location and Functional Impact of Pathogenic Variants

(A) Structure of MAPK1 complexed with a peptide from the D-motif of MKP3 (PDB: 2FYS). Different colors and representations highlight functional important regions. Activation segment, yellow; phosphorylatable residues Thr185 and Tyr187, red; helix C, light blue; mutated residues, semi-transparent violet surfaces; MKP3 D-motif, semi-transparent green surface; putative position of the second monomer in the MAPK1 dimer (according to PDB: 2ERK), gray surface. CD and ED domains, part of the DRS, are indicated. The ATP analog phosphoaminophosphonic acid-adenylate ester, not present in the structure, has been added in the corresponding position from the MAPK1/MNK1 complex (PDB: 2Y9Q) (orange sticks).

(B) Structures of MAPK1 complexes with peptides interacting with the DRS region, corresponding to D-motifs of phosphatases MKP3 (PDB: 2FYS) and PTPN7 (PDB: 2GPH), MAPK1 substrate MNK1 (PDB: 2Y9Q), and kinase MEK2 (PDB: 4H3Q). Representations and colors are used as above. The residues of the interacting peptides forming salt bridges with Asp318 are reported as sticks. In the case of MEK2, no residues form an ion pair with Asp318: the MEK2 residue closest to Asp318 is Arg4, whose side chain was not solved in the crystal structure, indicating that a stable salt bridge between MAPK1-Asp318 and MEK2-Arg4 residues is not present. A putative conformation for Arg4 has been modeled in the structure (thin sticks).

(C) Location and interactions of residues Ile74 and Ala174 in the active and inactive structures of MAPK1 (PDB: 2ERK and 1ERK, respectively). Representations and colors are used as above. Ile74, located on helix C, participates in a hydrophobic cluster comprising activation segment residues Ala171 and Val173, in both protein conformations. This region is critical in the activation mechanism. In the active state, Lys70 forms an ion pair with the phosphorylated Thr185, causing a remodeling of helix C, and the formation of a stronger salt bridge between conserved residues Glu71 and β3 Lys54, which is a prerequisite for activation. Ala174 is in the activation segment and interacts with Leu146, which is in the catalytic region. In all cases, residue numbers correspond to the human sequence.

the phosphorylatable residues Thr185 and Tyr187 are located. Interaction of the kinase with substrates, scaffolding proteins, and positive (MEK1/2) and negative (multiple MKPs) regulators is mediated by two other key regions, the D-site recruitment site (DRS) and F-site recruitment site (FRS).[47] Notably, substrates and regulators differentially use those domains to interact with the kinase.[58] In particular, the DRS binds to proteins with complementary D-motif linear sequences, and it contains a charged region and a hydrophobic groove. The charged region (termed the common docking [CD] domain) is an anionic patch comprising conserved key acidic residues (i.e., Asp318, Asp321 in MAPK1). The hydrophobic groove (Leu115, Leu121, Leu157, His125, Tyr128) is flanked by a more variable region (ED domain, Thr159, Thr160), important for binding selectivity.[58]

The affected residues were found to map at two specific regions of the kinase: His80, Asp318, Glu322, and Pro323 are part of or close to the DRS, while Ala174 is located on the activation segment and Ile74 interacts with it (Figure 5A). All residues are distant from the putative dimer interface, or from the FRS, and therefore are not predicted to affect the function of those regions. MAPK1 uses the DRS to bind to positive (i.e., MEK1/2) and negative (e.g., MKP3

and PTPN7) regulators, and a number of substrates (e.g., MNK1) (Figure 5B). MKP3, PTPN7, and MNK1 form a salt bridge interaction with Asp318 and interact with the other affected residues of this region (His80, Glu322, and Pro323). By contrast, the interface is much looser in the case of MEK2. Substitutions affecting residues in this region are thus predicted to affect the DRS affinity for signaling partners, with a weaker effect in the case of MEK2. This analysis is consistent with previous observations indicating that the p.Asp321Asn substitution in *X. laevis* (equivalent to p.Asp318Asn in the human protein) abolishes binding to MKP3 and MNK1, but only partially reduces association to MEK2.[59] Consistent with this, the equivalent substitution in the rat protein, p.Asp316Asn, causes a 10-fold decrease in the affinity for MKP3 and in the catalytic efficiency for the phosphorylation of ELK1 (but not of MBP, another ERK substrate).[60] Similarly, the cancer-associated p.Glu322Lys and p.Glu322Val (which are less conservative than the p.Glu322Gln amino acidic change reported here) are refractory to dephosphorylation by MKP3.[61]

In contrast, Ala174 is located within the activation segment, i.e., the region that drastically changes its conformation as a consequence of phosphorylation of Thr185 and Tyr187, causing activation of MAPK1 (Figure 5A). In addition, this residue is in contact with the catalytic site (and particularly with the conserved HRD motif) via a hydrophobic interaction with Leu146 (Figure 5C). Substitution with Val is predicted to perturb the allosteric switching of the activation segment. Finally, helix C, where Ile74 is located, has a central role in the activation of MAPK1. It comprises the conserved Glu71, which forms a salt bridge with the phosphate binding residue Lys54, stabilizing its position (Figure 5C).[57,62] Phosphorylation of Thr185 and Tyr187 promotes a conformational change of the activation lip that causes multiple interactions between Thr185 and helix C residues. In particular, in the active state, Lys70 and pThr185 form a salt bridge.[63] In turn, these interactions cause a remodeling of helix C, strengthening the Glu71-Lys54 ion pair and bringing catalytic residues in the correct alignment.[47,63] Residues of helix C, in particular Leu75, have also been implicated in the control of MAPK1 autophosphorylation, through the interaction with the "gatekeeper" residue Gln105.[64] Ile74 participates in a hydrophobic cluster comprising the activation segment residues Ala171 and Val173, and it is one helix turn away from conserved Glu71 and Lys70. Its substitution to a polar Asn residue is predicted to perturb the hydrophobic cluster and more in general the interactions of helix C with activation loop and catalytic site residues, which are crucial in the activation process.

To experimentally validate the hypothesis of a differential impact of the pathogenic MAPK1 amino acid substitutions on the binding properties of the kinase, we performed co-immunoprecipitation assays to assess binding of the mutants to MEK1 and MKP3. Experiments were carried out on lysates collected from HEK293T cells transiently transfected to co-express Xpress-tagged wild-type and mutant MAPK1 proteins together with Myc-tagged MEK1 or MKP3 (Figure 6A). Basally, the co-immunoprecipitated amount of all tested mutants with MEK1 was comparable to that of wild-type MAPK1, demonstrating that mutations do not significantly affect proper binding to the kinase. In contrast, all mutants were less efficiently immunoprecipitated by MKP3 following EGF stimulation compared to the wild-type protein, indicating a variably decreased binding to the phosphatase, with mutants carrying amino acid substitutions at the DRS having the most reduced binding. This finding was confirmed in primary fibroblasts endogenously expressing the p.Asp318Gly variant (Figure S6, left panel). Overall, the data indicate that the activating role of the disease-causing *MAPK1* variants is the result, at least in part, of a differential perturbed binding of the kinase with signaling partners.

MAPK1 Variation-Promoted Signaling Upregulation Retains Dependence on MEK Activity

The collected biochemical data indicated that the activating role of *MAPK1* variants is stimulus dependent, which raises the possibility that the aberrantly enhanced signaling driven by mutations might be druggable through MEK inhibition. To this goal, assays were performed to assess MAPK1, RSK, and MCL1 phosphorylation following treatment with trametinib, a well-known MEK1 inhibitor,[65] on transfected HEK293T cells overexpressing the MAPK1 mutants and primary fibroblasts heterozygous for the p.Asp318Gly change (Figures 6B and S6, right panel). Western blot analysis revealed a significant decrease of MAPK1, RSK, and MCL1 phosphorylation in EGF-stimulated transfected cells and fibroblasts after trametinib treatment, indicating a direct dependency of MAPK1 mutants on MEK1 to drive upregulated signaling through the MAPK cascade.

Discussion

Our findings establish germline *MAPK1* missense variants as the cause of a previously unrecognized neurodevelopmental disorder falling within the RASopathy clinical spectrum, with a phenotype reminiscent of NS in a subset of subjects. The non-random distribution of the identified allelic series and our *in silico*, *in vitro*, and *in vivo* data consistently indicate that pathogenic *MAPK1* variants cause GoF and promote a boosted signal flow through the MAPK cascade. The collected data suggest that the disease-causing amino acid changes can be subdivided into at least two major classes and offer a mechanistic interpretation for the activating consequences of variants affecting the DRS.

Although two individuals of the present cohort (subjects 1 and 2) were identified among a small cohort of subjects with features suggestive of NS for whom pathogenic variants had not been identified in known RASopathy-associated genes, systematic screening of the entire *MAPK1* coding sequence in an additional 267 subjects who had a clinically suspected diagnosis of RASopathy not explained

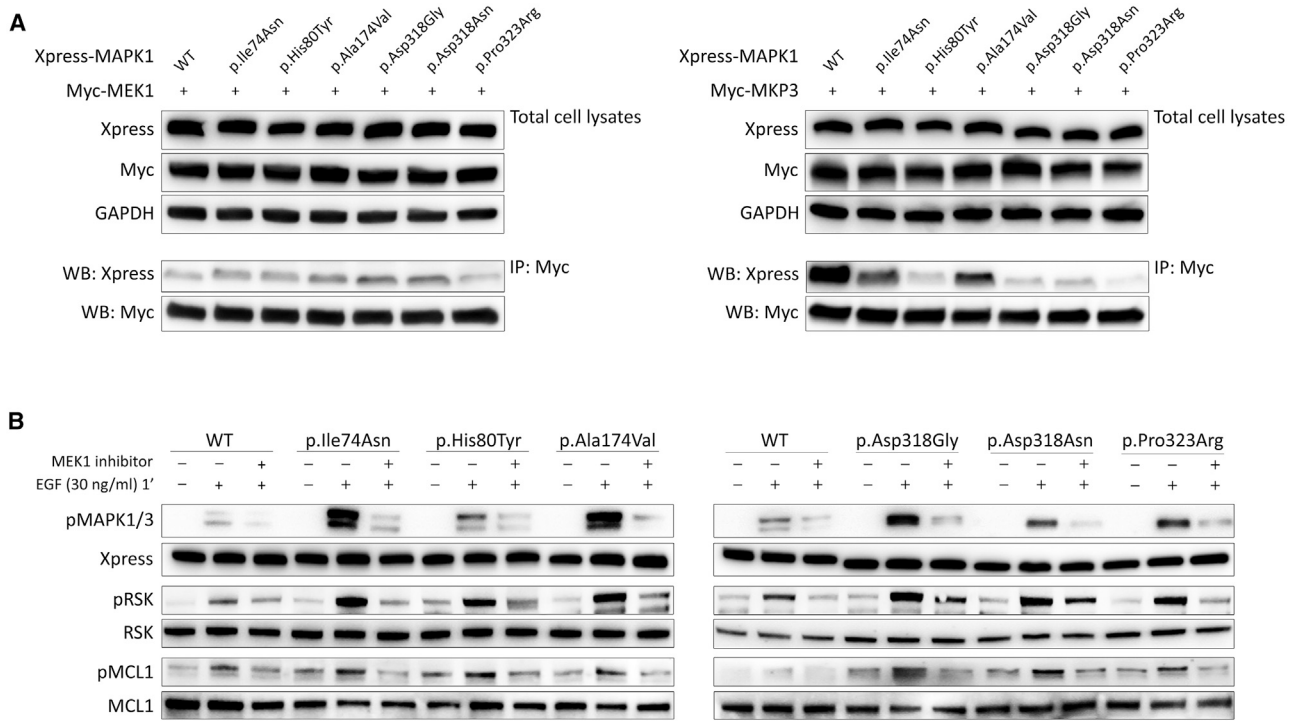

Figure 6. Disease-Causing Mutations Impair Binding of MAPK1 with MKP3 but Not Binding to MEK1, and Retain Dependence on MEK Activity in Their Upregulation of MAPK Signaling

(A) Co-immunoprecipitation assays. Lysates from HEK293T cells transiently transfected to express wild-type and mutant Xpress-tagged MAPK1 protein with Myc-MEK1 or Myc-MKP3 were immunoprecipitated with an anti-Myc antibody and assayed by western blotting using the indicated antibodies.

(B) *MAPK1* mutation-promoted MAPK signal upregulation retains dependence on MEK activity. MAPK, RSK, and MCL1 phosphorylation assays were performed in transiently transfected HEK293T cells starved for 16 h and stimulated with EGF (30 ng/mL, 1 min) after treatment with the MEK inhibitor trametinib (1.5 ng/mL for 2 h). Blots show a decrease in pMAPK, pRSK and pMCL1 in cells overexpressing wild-type or mutant MAPK1 proteins in presence of trametinib, indicating that the mutation-driven signal upregulation of the MAPK cascade retains dependence on MEK activity.

by mutations in the previously identified genes implicated in these disorders did not find other pathogenic variants. This suggests that *MAPK1* variation represents a rare event in subjects with NS-related features and that it may be more commonly associated with currently unclassified syndromic DD/ID.

Our collective data indicate that pathogenic *MAPK1* variants are activating and can be classified within two mechanistic groups affecting proper binding of the kinase to regulators and effectors or perturbing the mechanism of activation of the kinase. We showed that the defective negative regulation exerted by MKP3 (and possibly other MKPs) represents a generalizable mechanism for the GoF behavior of the identified *MAPK1* variants. Notably, substitutions in or close to the DRS can lead to either GoF or LoF[61] by impairing proper MAPK1 binding to regulators and substrates. Our structural and experimental analyses support a model in which disease-causing variants operate with counteracting effects on MAPK1 function by differentially impacting the ability of the altered proteins to interact with MEK1, MKP3, and substrates. Remarkably, the evidence that only some intermolecular interactions are impaired by the pathogenic substitutions in the DRS strongly suggests that these lesions produce only a local perturbation of the binding interface, rather than an overall conformational rearrangement of the CD domain. Consistent with the GoF role of the identified *MAPK1* variants, no pathogenic amino acid change was found to involve residues at the FRS. This is in line with recent data demonstrating a mutually exclusive distribution of GoF and LoF *MAPK1* changes in these domains, with the former limited to DRS residues and the latter involving FRS residues.[61]

According to the Tissue Cancer Genome Atlas and Cosmic datasets, *MAPK1* gene amplification is observed in a significant proportion of ovarian, bladder, lung, and breast cancers (5% to 20% of cases). However, while enhanced MAPK1 activation driven by oncogenic mutations in upstream signal transducers (e.g., *PTPN11*, *HRAS* [MIM: 190020], *KRAS* [MIM: 190070], *NRAS* [MIM: 164790], and *BRAF* [MIM: 164757]) is a common theme in cancer, *MAPK1* mutations do not represent a major somatic event contributing to oncogenesis. Indeed, they have been reported in a substantially restricted number of tumors and less frequently with respect to other genes coding for signal transducers with role in the RAS-MAPK pathway (COSMIC database). Based on our findings, this is likely linked to the particular behavior of these mutations, which are stimulus dependent and confer only mild and/or context-specific

GoF because of their counterbalancing consequences on MAPK1 function. In this proposed model, the disease-causing amino acid substitutions clustering at the DRS significantly affect MKP3 binding and MKP3-mediated MAPK1 dephosphorylation of the regulatory residues, Thr185 and Tyr187. However, since DRS also mediates MAPK1 binding to a number of signaling partners and scaffolding proteins, it is possible that these mutations may also variably impact binding of the kinase to a large number of MAPK1 interacting proteins, including substrates.[47,60,66,67] It is therefore reasonable to hypothesize that each of the identified pathogenic variants may variably exert counterbalancing effects on the phosphorylation status of the kinase and its capability to couple its activation to efficient phosphorylation of substrates.

We clinically and molecularly profile a RASopathy caused by activating germline pathogenic variation of *MAPK1*. After nearly 20 years from the discovery of the first gene implicated in NS, *PTPN11*,[15] the last tier of the MAPK cascade finally joins the group of genes mutated in RASopathies. Our findings further extend the molecular mechanisms by which upregulation of MAPK signaling is linked to human disease and provide a rationale for the differential impact of *MAPK1* mutations in development and oncogenesis.

Data and Code Availability

The pathogenic variants identified in this work have been submitted to ClinVar under the following accession numbers: c.221T>A, SCV001337682; c.238C>T, SCV001337683; c.521C>T, SCV001337684; c.952G>A, SCV001337685; c.953A>G, SCV001337686; c.964G>C, SCV001337687; c.968C>G, SCV001337688. WES datasets have not been deposited in a public repository due to privacy and ethical restrictions but are available from the corresponding author on request.

Supplemental Data

Supplemental Data can be found online at https://doi.org/10.1016/j.ajhg.2020.06.018.

Acknowledgments

The authors thank the subjects and their families for participating in this study. We are grateful to Shin Takagi (University of Nagoya, Japan) and James D. McGhee (University of Calgary, Canada) for providing the original plasmids used for *C. elegans* studies, and Serenella Venanzi (Istituto Superiore di Sanità, Rome, Italy) and Rosalba Carrozzo (Ospedale Pediatrico Bambino Gesù, Rome, Italy) for technical assistance. *C. elegans* strains were provided by the CGC, which is funded by NIH Office of Research Infrastructure Programs (P40 OD010440). This work was supported by grants from EJP-RD (NSEuroNet) to M.Z. and M.T. and by AIRC (IG 21614) and Ministero della Salute (Ricerca Corrente 2019, 2020) to M.T. Funding from the JPB Foundation was provided to W.K.C.

Declaration of Interests

I.M.W. and M.M.M. are employees of GeneDx. S.Á. and M.M.-G. are employees of NimGenetics. All the other authors declare no competing interests.

Received: May 13, 2020
Accepted: June 24, 2020
Published: July 27, 2020

Web Resources

ClinVar, https://www.ncbi.nlm.nih.gov/clinvar/
COSMIC, http://cancer.sanger.ac.uk/cosmic/signatures
ExAC Browser, http://exac.broadinstitute.org/
GenBank, https://www.ncbi.nlm.nih.gov/genbank/
Gene SeT AnaLysis, http://www.webgestalt.org/option.php
gnomAD Browser, https://gnomad.broadinstitute.org/
InterVar, http://wintervar.wglab.org
OMIM, https://www.omim.org/
RCSB Protein Data Bank, http://www.rcsb.org/pdb/home/home.do
UMCUGenetics/IAP, https://github.com/UMCUGenetics/IAP/tree/v2.2.0

References

1. Yoon, S., and Seger, R. (2006). The extracellular signal-regulated kinase: multiple substrates regulate diverse cellular functions. Growth Factors *24*, 21–44.
2. Kolch, W. (2005). Coordinating ERK/MAPK signalling through scaffolds and inhibitors. Nat. Rev. Mol. Cell Biol. *6*, 827–837.
3. Samatar, A.A., and Poulikakos, P.I. (2014). Targeting RAS-ERK signalling in cancer: promises and challenges. Nat. Rev. Drug Discov. *13*, 928–942.
4. Krens, S.F., Spaink, H.P., and Snaar-Jagalska, B.E. (2006). Functions of the MAPK family in vertebrate-development. FEBS Lett. *580*, 4984–4990.
5. Hayashi, S., and Ogura, Y. (2020). ERK signaling dynamics in the morphogenesis and homeostasis of Drosophila. Curr. Opin. Genet. Dev. *63*, 9–15.
6. Thomas, G.M., and Huganir, R.L. (2004). MAPK cascade signalling and synaptic plasticity. Nat. Rev. Neurosci. *5*, 173–183.
7. Tartaglia, M., and Gelb, B.D. (2010). Disorders of dysregulated signal traffic through the RAS-MAPK pathway: phenotypic spectrum and molecular mechanisms. Ann. N Y Acad. Sci. *1214*, 99–121.
8. Rauen, K.A. (2013). The RASopathies. Annu. Rev. Genomics Hum. Genet. *14*, 355–369.
9. Aoki, Y., Niihori, T., Inoue, S., and Matsubara, Y. (2016). Recent advances in RASopathies. J. Hum. Genet. *61*, 33–39.
10. Kratz, C.P., Franke, L., Peters, H., Kohlschmidt, N., Kazmierczak, B., Finckh, U., Bier, A., Eichhorn, B., Blank, C., Kraus, C., et al. (2015). Cancer spectrum and frequency among children with Noonan, Costello, and cardio-facio-cutaneous syndromes. Br. J. Cancer *112*, 1392–1397.
11. Dunnett-Kane, V., Burkitt-Wright, E., Blackhall, F.H., Malliri, A., Evans, D.G., and Lindsay, C.R. (2020). Germline and sporadic cancers driven by the RAS pathway: parallels and contrasts. Ann. Oncol. *31*, 873–883.

12. Villani, A., Greer, M.C., Kalish, J.M., Nakagawara, A., Nathanson, K.L., Pajtler, K.W., Pfister, S.M., Walsh, M.F., Wasserman, J.D., Zelley, K., and Kratz, C.P. (2017). Recommendations for Cancer Surveillance in Individuals with RASopathies and Other Rare Genetic Conditions with Increased Cancer Risk. Clin. Cancer Res. *23*, e83–e90.
13. Simanshu, D.K., Nissley, D.V., and McCormick, F. (2017). RAS proteins and their regulators in human disease. Cell *170*, 17–33.
14. Roberts, A.E., Allanson, J.E., Tartaglia, M., and Gelb, B.D. (2013). Noonan syndrome. Lancet *381*, 333–342.
15. Tartaglia, M., Mehler, E.L., Goldberg, R., Zampino, G., Brunner, H.G., Kremer, H., van der Burgt, I., Crosby, A.H., Ion, A., Jeffery, S., et al. (2001). Mutations in PTPN11, encoding the protein tyrosine phosphatase SHP-2, cause Noonan syndrome. Nat. Genet. *29*, 465–468.
16. Tartaglia, M., Pennacchio, L.A., Zhao, C., Yadav, K.K., Fodale, V., Sarkozy, A., Pandit, B., Oishi, K., Martinelli, S., Schackwitz, W., et al. (2007). Gain-of-function SOS1 mutations cause a distinctive form of Noonan syndrome. Nat. Genet. *39*, 75–79.
17. Roberts, A.E., Araki, T., Swanson, K.D., Montgomery, K.T., Schiripo, T.A., Joshi, V.A., Li, L., Yassin, Y., Tamburino, A.M., Neel, B.G., and Kucherlapati, R.S. (2007). Germline gain-of-function mutations in SOS1 cause Noonan syndrome. Nat. Genet. *39*, 70–74.
18. Pandit, B., Sarkozy, A., Pennacchio, L.A., Carta, C., Oishi, K., Martinelli, S., Pogna, E.A., Schackwitz, W., Ustaszewska, A., Landstrom, A., et al. (2007). Gain-of-function RAF1 mutations cause Noonan and LEOPARD syndromes with hypertrophic cardiomyopathy. Nat. Genet. *39*, 1007–1012.
19. Razzaque, M.A., Nishizawa, T., Komoike, Y., Yagi, H., Furutani, M., Amo, R., Kamisago, M., Momma, K., Katayama, H., Nakagawa, M., et al. (2007). Germline gain-of-function mutations in RAF1 cause Noonan syndrome. Nat. Genet. *39*, 1013–1017.
20. Aoki, Y., Niihori, T., Banjo, T., Okamoto, N., Mizuno, S., Kurosawa, K., Ogata, T., Takada, F., Yano, M., Ando, T., et al. (2013). Gain-of-function mutations in RIT1 cause Noonan syndrome, a RAS/MAPK pathway syndrome. Am. J. Hum. Genet. *93*, 173–180.
21. Yamamoto, G.L., Aguena, M., Gos, M., Hung, C., Pilch, J., Fahiminiya, S., Abramowicz, A., Cristian, I., Buscarilli, M., Naslavsky, M.S., et al. (2015). Rare variants in SOS2 and LZTR1 are associated with Noonan syndrome. J. Med. Genet. *52*, 413–421.
22. Johnston, J.J., van der Smagt, J.J., Rosenfeld, J.A., Pagnamenta, A.T., Alswaid, A., Baker, E.H., Blair, E., Borck, G., Brinkmann, J., Craigen, W., et al.; Members of the Undiagnosed Diseases Network (2018). Autosomal recessive Noonan syndrome associated with biallelic LZTR1 variants. Genet. Med. *20*, 1175–1185.
23. Bauer, C.K., Calligari, P., Radio, F.C., Caputo, V., Dentici, M.L., Falah, N., High, F., Pantaleoni, F., Barresi, S., Ciolfi, A., et al. (2018). Mutations in KCNK4 that affect gating cause a recognizable neurodevelopmental syndrome. Am. J. Hum. Genet. *103*, 621–630.
24. Flex, E., Martinelli, S., Van Dijck, A., Ciolfi, A., Cecchetti, S., Coluzzi, E., Pannone, L., Andreoli, C., Radio, F.C., Pizzi, S., et al. (2019). Aberrant Function of the C-Terminal Tail of HIST1H1E Accelerates Cellular Senescence and Causes Premature Aging. Am. J. Hum. Genet. *105*, 493–508.
25. Magini, P., Smits, D.J., Vandervore, L., Schot, R., Columbaro, M., Kasteleijn, E., van der Ent, M., Palombo, F., Lequin, M.H., Dremmen, M., et al. (2019). Loss of SMPD4 Causes a Developmental Disorder Characterized by Microcephaly and Congenital Arthrogryposis. Am. J. Hum. Genet. *105*, 689–705.
26. Thevenon, J., Duffourd, Y., Masurel-Paulet, A., Lefebvre, M., Feillet, F., El Chehadeh-Djebbar, S., St-Onge, J., Steinmetz, A., Huet, F., Chouchane, M., et al. (2016). Diagnostic odyssey in severe neurodevelopmental disorders: toward clinical whole-exome sequencing as a first-line diagnostic test. Clin. Genet. *89*, 700–707.
27. Miller, C.R., Lee, K., Pfau, R.B., Reshmi, S.C., Corsmeier, D.J., Hashimoto, S., Dave-Wala, A., Jayaraman, V., Koboldt, D., Matthews, T., et al. (2020). Disease-associated mosaic variation in clinical exome sequencing: a two-year pediatric tertiary care experience. Cold Spring Harb. Mol. Case Stud. *6*, a005231.
28. Retterer, K., Juusola, J., Cho, M.T., Vitazka, P., Millan, F., Gibellini, F., Vertino-Bell, A., Smaoui, N., Neidich, J., Monaghan, K.G., et al. (2016). Clinical application of whole-exome sequencing across clinical indications. Genet. Med. *18*, 696–704.
29. Rodríguez, C., Sánchez-Morán, I., Álvarez, S., Tirado, P., Fernández-Mayoralas, D.M., Calleja-Pérez, B., Almeida, Á., and Fernández-Jaén, A. (2019). A novel human Cdh1 mutation impairs anaphase promoting complex/cyclosome activity resulting in microcephaly, psychomotor retardation, and epilepsy. J. Neurochem. *151*, 103–115.
30. Martinelli, S., Torreri, P., Tinti, M., Stella, L., Bocchinfuso, G., Flex, E., Grottesi, A., Ceccarini, M., Palleschi, A., Cesareni, G., et al. (2008). Diverse driving forces underlie the invariant occurrence of the T42A, E139D, I282V and T468M SHP2 amino acid substitutions causing Noonan and LEOPARD syndromes. Hum. Mol. Genet. *17*, 2018–2029.
31. Motta, M., Chillemi, G., Fodale, V., Cecchetti, S., Coppola, S., Stipo, S., Cordeddu, V., Macioce, P., Gelb, B.D., and Tartaglia, M. (2016). SHOC2 subcellular shuttling requires the KEKE motif-rich region and N-terminal leucine-rich repeat domain and impacts on ERK signalling. Hum. Mol. Genet. *25*, 3824–3835.
32. Motta, M., Fidan, M., Bellacchio, E., Pantaleoni, F., Schneider-Heieck, K., Coppola, S., Borck, G., Salviati, L., Zenker, M., Cirstea, I.C., and Tartaglia, M. (2019). Dominant Noonan syndrome-causing LZTR1 mutations specifically affect the Kelch domain substrate-recognition surface and enhance RAS-MAPK signaling. Hum. Mol. Genet. *28*, 1007–1022.
33. Kaboord, B., and Perr, M. (2008). Isolation of proteins and protein complexes by immunoprecipitation. Methods Mol. Biol. *424*, 349–364.
34. Sulston, J.E., and Hodgkin, J. (1988). Methods. In The Nematode *Caenorhabditis elegans*, W.B. Wood, ed. (Cold Spring Harbor, NY: Cold Spring Harbor Laboratory Press), pp. 587–606.
35. Mello, C.C., Kramer, J.M., Stinchcomb, D., and Ambros, V. (1991). Efficient gene transfer in C.elegans: extrachromosomal maintenance and integration of transforming sequences. EMBO J. *10*, 3959–3970.
36. Aroian, R.V., and Sternberg, P.W. (1991). Multiple functions of let-23, a Caenorhabditis elegans receptor tyrosine kinase gene required for vulval induction. Genetics *128*, 251–267.
37. Aroian, R.V., Lesa, G.M., and Sternberg, P.W. (1994). Mutations in the Caenorhabditis elegans let-23 EGFR-like gene define elements important for cell-type specificity and function. EMBO J. *13*, 360–366.

38. Paix, A., Folkmann, A., Rasoloson, D., and Seydoux, G. (2015). High Efficiency, Homology-Directed Genome Editing in Caenorhabditis elegans Using CRISPR-Cas9 Ribonucleoprotein Complexes. Genetics *201*, 47–54.
39. Pettersen, E.F., Goddard, T.D., Huang, C.C., Couch, G.S., Greenblatt, D.M., Meng, E.C., and Ferrin, T.E. (2004). UCSF Chimera–a visualization system for exploratory research and analysis. J. Comput. Chem. *25*, 1605–1612.
40. Shapovalov, M.V., and Dunbrack, R.L., Jr. (2011). A smoothed backbone-dependent rotamer library for proteins derived from adaptive kernel density estimates and regressions. Structure *19*, 844–858.
41. Lek, M., Karczewski, K.J., Minikel, E.V., Samocha, K.E., Banks, E., Fennell, T., O'Donnell-Luria, A.H., Ware, J.S., Hill, A.J., Cummings, B.B., et al.; Exome Aggregation Consortium (2016). Analysis of protein-coding genetic variation in 60,706 humans. Nature *536*, 285–291.
42. Sobreira, N., Schiettecatte, F., Valle, D., and Hamosh, A. (2015). GeneMatcher: a matching tool for connecting investigators with an interest in the same gene. Hum. Mutat. *36*, 928–930.
43. Ioannidis, N.M., Rothstein, J.H., Pejaver, V., Middha, S., McDonnell, S.K., Baheti, S., Musolf, A., Li, Q., Holzinger, E., Karyadi, D., et al. (2016). REVEL: An Ensemble Method for Predicting the Pathogenicity of Rare Missense Variants. Am. J. Hum. Genet. *99*, 877–885.
44. Kircher, M., Witten, D.M., Jain, P., O'Roak, B.J., Cooper, G.M., and Shendure, J. (2014). A general framework for estimating the relative pathogenicity of human genetic variants. Nat. Genet. *46*, 310–315.
45. Wiel, L., Venselaar, H., Veltman, J.A., Vriend, G., and Gilissen, C. (2017). Aggregation of population-based genetic variation over protein domain homologues and its potential use in genetic diagnostics. Hum. Mutat. *38*, 1454–1463.
46. Li, Q., and Wang, K. (2017). InterVar: Clinical interpretation of genetic variants by ACMG-AMP 2015 guidelines. Am. J. Hum. Genet. *100*, 267–280.
47. Roskoski, R., Jr. (2012). ERK1/2 MAP kinases: structure, function, and regulation. Pharmacol. Res. *66*, 105–143.
48. Maik-Rachline, G., Hacohen-Lev-Ran, A., and Seger, R. (2019). Nuclear ERK: Mechanism of Translocation, Substrates, and Role in Cancer. Int. J. Mol. Sci. *20*, 1194.
49. Plotnikov, A., Chuderland, D., Karamansha, Y., Livnah, O., and Seger, R. (2019). Nuclear ERK translocation is mediated by protein kinase CK2 and accelerated by autophosphorylation. Cell. Physiol. Biochem. *53*, 366–387.
50. Marais, R., Wynne, J., and Treisman, R. (1993). The SRF accessory protein Elk-1 contains a growth factor-regulated transcriptional activation domain. Cell *73*, 381–393.
51. Gille, H., Kortenjann, M., Thomae, O., Moomaw, C., Slaughter, C., Cobb, M.H., and Shaw, P.E. (1995). ERK phosphorylation potentiates Elk-1-mediated ternary complex formation and transactivation. EMBO J. *14*, 951–962.
52. Sundaram, M.V. (2013). Canonical RTK-Ras-ERK signaling and related alternative pathways, WormBook, ed. The C. elegans Research Community, WormBook, http://www.wormbook.org.
53. Sternberg, P.W. (2005). Vulval development, WormBook, ed. The C. elegans Research Community, http://www.wormbook.org.
54. Lackner, M.R., and Kim, S.K. (1998). Genetic analysis of the Caenorhabditis elegans MAP kinase gene mpk-1. Genetics *150*, 103–117.
55. Lackner, M.R., Kornfeld, K., Miller, L.M., Horvitz, H.R., and Kim, S.K. (1994). A MAP kinase homolog, mpk-1, is involved in ras-mediated induction of vulval cell fates in Caenorhabditis elegans. Genes Dev. *8*, 160–173.
56. Wu, Y., and Han, M. (1994). Suppression of activated Let-60 ras protein defines a role of Caenorhabditis elegans Sur-1 MAP kinase in vulval differentiation. Genes Dev. *8*, 147–159.
57. Zhang, F., Strand, A., Robbins, D., Cobb, M.H., and Goldsmith, E.J. (1994). Atomic structure of the MAP kinase ERK2 at 2.3 A resolution. Nature *367*, 704–711.
58. Sammons, R.M., Ghose, R., Tsai, K.Y., and Dalby, K.N. (2019). Targeting ERK beyond the boundaries of the kinase active site in melanoma. Mol. Carcinog. *58*, 1551–1570.
59. Tanoue, T., Adachi, M., Moriguchi, T., and Nishida, E. (2000). A conserved docking motif in MAP kinases common to substrates, activators and regulators. Nat. Cell Biol. *2*, 110–116.
60. Zhang, J., Zhou, B., Zheng, C.F., and Zhang, Z.Y. (2003). A bipartite mechanism for ERK2 recognition by its cognate regulators and substrates. J. Biol. Chem. *278*, 29901–29912.
61. Brenan, L., Andreev, A., Cohen, O., Pantel, S., Kamburov, A., Cacchiarelli, D., Persky, N.S., Zhu, C., Bagul, M., Goetz, E.M., et al. (2016). Phenotypic characterization of a comprehensive set of MAPK1/ERK2 missense mutants. Cell Rep. *17*, 1171–1183.
62. Roskoski, R., Jr. (2015). A historical overview of protein kinases and their targeted small molecule inhibitors. Pharmacol. Res. *100*, 1–23.
63. Canagarajah, B.J., Khokhlatchev, A., Cobb, M.H., and Goldsmith, E.J. (1997). Activation mechanism of the MAP kinase ERK2 by dual phosphorylation. Cell *90*, 859–869.
64. Emrick, M.A., Lee, T., Starkey, P.J., Mumby, M.C., Resing, K.A., and Ahn, N.G. (2006). The gatekeeper residue controls autoactivation of ERK2 via a pathway of intramolecular connectivity. Proc. Natl. Acad. Sci. USA *103*, 18101–18106.
65. Gilmartin, A.G., Bleam, M.R., Groy, A., Moss, K.G., Minthorn, E.A., Kulkarni, S.G., Rominger, C.M., Erskine, S., Fisher, K.E., Yang, J., et al. (2011). GSK1120212 (JTP-74057) is an inhibitor of MEK activity and activation with favorable pharmacokinetic properties for sustained in vivo pathway inhibition. Clin. Cancer Res. *17*, 989–1000.
66. Sharrocks, A.D., Yang, S.H., and Galanis, A. (2000). Docking domains and substrate-specificity determination for MAP kinases. Trends Biochem. Sci. *25*, 448–453.
67. Peti, W., and Page, R. (2013). Molecular basis of MAP kinase regulation. Protein Sci. *22*, 1698–1710.

The American Journal of Human Genetics, Volume *107*

Supplemental Data

Enhanced MAPK1 Function Causes a Neurodevelopmental Disorder within the RASopathy Clinical Spectrum

Marialetizia Motta, Luca Pannone, Francesca Pantaleoni, Gianfranco Bocchinfuso, Francesca Clementina Radio, Serena Cecchetti, Andrea Ciolfi, Martina Di Rocco, Mariet W. Elting, Eva H. Brilstra, Stefania Boni, Laura Mazzanti, Federica Tamburrino, Larry Walsh, Katelyn Payne, Alberto Fernández-Jaén, Mythily Ganapathi, Wendy K. Chung, Dorothy K. Grange, Ashita Dave-Wala, Shalini C. Reshmi, Dennis W. Bartholomew, Danielle Mouhlas, Giovanna Carpentieri, Alessandro Bruselles, Simone Pizzi, Emanuele Bellacchio, Francesca Piceci-Sparascio, Christina Lißewski, Julia Brinkmann, Ronald R. Waclaw, Quinten Waisfisz, Koen van Gassen, Ingrid M. Wentzensen, Michelle M. Morrow, Sara Álvarez, Mónica Martínez-García, Alessandro De Luca, Luigi Memo, Giuseppe Zampino, Cesare Rossi, Marco Seri, Bruce D. Gelb, Martin Zenker, Bruno Dallapiccola, Lorenzo Stella, Carlos E. Prada, Simone Martinelli, Elisabetta Flex, and Marco Tartaglia

SUPPLEMENTAL DATA

Case Reports

Figure S1. Multiple protein sequence alignment among MAPK1 orthologs and MAPK3.

Figure S2. Tolerance landscape of genetic variation for *MAPK1*.

Figure S3. The evolving phenotype of Subject 2 with age.

Figure S4. MAPK and RSK phosphorylation assays performed in primary fibroblasts from Subject 2 (p.Asp318Gly).

Figure S5. RASopathy-causing MAPK1 proteins show a variably enhanced nuclear translocation in response to EGF stimulation.

Figure S6. Endogenous MAPK1^{D318G} less efficiently co-immunoprecipitates with MKP3 and retains dependence on MEK activity in upregulating MAPK signaling.

Table S1. WES info and statistics.

Table S2. WES data output.

Table S3. Clinical features of subjects with *de novo* pathogenic *MAPK1* variants.

Table S4. Vulval phenotypes in *mpk-1*(*pan14*[D321G]) knock-in *C. elegans* hermaphrodites and in worms overexpressing a subset of disease-causing *MAPK1* mutant alleles under the control of p*lin-31*.

Case Reports

Subject 1 (p.Ala174Val), a male, is the only child of healthy, non-consanguineous Italian parents. The age of parents at birth was 30 years. Family history was unremarkable. He has one healthy half-sister (21 years old) and one half-brother (4 years old). He was born at 41 weeks of gestation by Cesarean section after an uneventful pregnancy. Birth weight was 3,650 g (+0.6 SD) and length 53 cm (+1.65 SD). OFC and Apgar scores were not available. Perinatal period was normal. Developmental milestones were mildly delayed (he walked alone at 18 months, first words reported at 12 months). He presented fine motor delay and atypical social behaviors characterized by anxiety and reduced stress tolerance. At 6 years, mitral regurgitation with mitral valve prolapse and patent foramen ovale was noted. Clinical evaluation at 13 years disclosed curly and thick hair, epicanthal folds, mild hypertelorism, blue eyes, low-set posteriorly rotated ears, multiple lentigines, pterygium colli, scapular winging, cubitus valgus, and bilateral pes planus. He has myopia corrected with lens. At the last evaluation, the height was 157 cm (-0.04 SD), weight 45.5 kg (-0.01 SD) and OFC 59 cm (+2.82 SD). Extensive genetic analyses, including array-CGH and a large panel of RASopathy genes, were normal.

Subject 2 (p.Asp318Gly) was born at 40 weeks of gestation following an uneventful pregnancy and delivery. Birth weight was 3,350 g (-0.6 SD), length 47 cm (-2.28 SD), head circumference 33 cm (-1.75 SD). The parents were not consanguineous, and the family history was unremarkable. Neonatal transition was normal. At 2 years, he was referred to our unit for growth retardation and mild psychomotor delay. Physical examination revealed brachicephaly, hypertelorism, epicanthal folds, downslanting palpebral fissures, bilateral ptosis, low-set posteriorly rotated ears, wide nasal bridge, prominent and pointed chin, a low posterior hairline, mild hypotonia, one cafè-au-lait spot, and three hypochromic spots. Peripheral lymphedema was also observed. Echocardiography showed an atrial septal defect, which later resolved spontaneously and mild mitral valve prolapse, which was not hemodynamically relevant. Abdominal and renal sonography were normal. He had mild psychomotor delay, moderate intellectual disability with a learning disorder and graphomotor and praxic constructive skills deficit. He received rehabilitative physical therapy and speech therapy. Pharmacological therapy was also administered to treat his ADHD. Cerebral MRI showed cavum septum pellucidum. Results of ophthalmologic and ENT evaluations were normal. He presented with bilateral pes planus and mild legs asymmetry (5 mm). He underwent surgery for monolateral cryptorchidism and hypospadia. At age 3 years, partial GH deficiency was diagnosed, and he was treated with GH therapy. At the auxological follow-up (12 years), height had increased to 25th centile and the pubertal growth spurt had started.

Subject 3 (p.His80Tyr), a male, was born at 39 weeks of gestation. The pregnancy had been complicated by slightly increased nuchal translucency (3.8 mm at 12 weeks). Amniocentesis showed a normal karyotype. Birth weight was 3,672 g (+0.5 SD), length 50 cm (0 SD), head circumference 34.5 cm (0 SD), APGAR score 8/10/10 at 1, 5 and 10 minutes, respectively. The neonatal period had been complicated by transient tachypnea and feeding problems that required tube feeding for one month. At 1 month of age, brain MRI showed mild widening of frontal peripheral fluid spaces. A suspicion of seizures was ruled out by a normal EEG pattern. Developmental milestones were delayed (rolled over at 9 months, sit almost independently at 12 months, crawling at 18 months, walking at 30 months). Sleeping problems had already been recorded at 6 months. Speech was delayed

at 2 years of age. He had chronic middle ear effusions and received ear tubes. Audiologic investigations were difficult, because of behavioral problems but did not show hearing loss. Clinical evaluation at 6 years of age revealed frustrated and aggressive behavior, head-banging, spitting and hitting, language delay (few words, no sentences) and an easy bruising. He was diagnosed with celiac disease. Growth parameters were impaired (height: 105 cm, -3 SD; weight: 17.4 kg, -2 SD; OFC: 48.5 cm; -2 SD). The dysmorphological evaluation evidenced a high forehead, medially thin and flaring eyebrows, posteriorly rotated ears, round nasal tip, upturned nostrils, small teeth with fusion of two teeth, broad thorax, flat feet and bruises at arms and legs. The follow-up evaluation at 9 years of age confirmed the intellectual disability and language delay (few words). Behavior problems were confirmed, although slightly improved. He had a dry skin (especially at the back of upper arms). No heart malformation was detected by echocardiography at 6 years of age. Genetic and metabolic testing including Prader-Willi syndrome methylation profile, chromosomal microarray, UPD14 and fragile X-syndrome were normal.

Subject 4 (p.Asp318Asn) is a 17 year-old female, first child of healthy non-consanguineous Dutch parents. Premature rupture of the membranes occurred at 30 weeks gestation, but pregnancy was otherwise normal. A Caesarean section was performed (37 weeks of gestation) because of breech position. Birth weight was 2,610 g (10th-50th centile). Length, OFC and Apgar scores were not available. Perinatal period was uncomplicated. Developmental milestones were delayed. She walked independently when she was 20 months old. At 3 years, she spoke single words only. Ear tubes were inserted and speech therapy was initiated. By age 4, she used 3 to 4 words per sentence, but her speech was difficult to understand. At the age of 9 years, her total IQ score was 64, with a verbal IQ of 71 and a nonverbal IQ of 61. She could read and write some words, and could get dressed and eat independently. She attends a school for special education. She was diagnosed with ADHD, which has been treated with methylphenidate. At the age of 16 years, Tietze syndrome was diagnosed. Clinical evaluation disclosed a broad forehead, dark broad horizontal eyebrows, hypertelorism, short and almond-shaped palpebral fissures, thick vermillion of the upper and lower lip, slightly posterior rotated ears, low posterior hairline, hypertrichosis, a broad thorax and a hoarse voice. At the last evaluation, her height was 163 cm (-0.87 SD) and weight was 53.5 kg (-0.5 SD). Echocardiography showed mitral valve billowing. Biochemical and metabolic screening were normal, as was testing of *FMR1* and *ABCC9.* Array-CGH revealed a paternally inherited duplication of 2q12.3q13 (~310 Kb).

Subject 5 (p.Pro323Arg) was a male born at 41 weeks gestational age *via* SVD after uncomplicated pregnancy. Mother was a 37 year-old G5P4 and father was 40 years old. He had a normal newborn metabolic screen. He was diagnosed with an atrial septal defect by echocardiogram. At 4 months of age, he presented with seizures and was admitted to the hospital. EEG was consistent with infantile spasms. He was treated with vigabatrin with good response. At age 1 year, he has been seizure free with a normal repeated EEG. At 4 months, brain MRI did not identify congenital malformations. The patient had multiple admissions for pneumonia, later on diagnosed with aspiration culture. A gastrostomy tube was placed at 14 months. He is primarily fed via this tube but can eat solids and thickened liquids by mouth. He was also diagnosed with a right duplicated kidney collecting system by ultrasound. Developmental delay was suspected at age 8 months. He rolled over at age 8 months, sat unassisted at age 10 months, crawled at 19 months, and walked at 27 months. He has few words and was diagnosed with speech apraxia. He also has difficulty

in communication and interaction and has an aggressive behavior. He cannot sit still for any period, and is not interested in socializing. Behavior is in the autism spectrum disorder, which is treated with ABA therapy. No sleep difficulties have been reported. He is not toilet trained yet. Genetic testing, including SNP chromosomal microarray, lysosomal studies, and urine studies for organic acids and mucopolysaccharides provided normal results.

Subject 6 (p.Glu322Gln), a male, is the third child of healthy parents. At birth he came to medical attention because of multiple dysmorphic features including bilateral clubfeet, hypotonia, ptosis and cryptorchidism, though no genetic testing was performed. He was the 3,060 g product of a 38 weeks gestation born *via* SVD to a 26-year-old G3P3 female whose pregnancy was said to be uncomplicated. He was evaluated at 2 years for his very poor growth and global delays and again at age 5, when he underwent testing to include a chromosomal microarray, serum 7-DHC, PWS methylation testing, metabolic studies and a Noonan syndrome gene panel, all of which were normal. The parents were told that the child likely had a form of Noonan syndrome. He has been lost to genetics follow-up until 2019 when he underwent a new evaluation, primarily due to parental concern about Crohn's disease affecting growth at age 15. Examination at that time revealed severe growth retardation with all parameters measuring well below the 1st percentile. Dysmorphic features included trigonocephalic skull, large pinnae with superior protrusion and posterior rotation, severe bilateral ptosis with downslanting palpebral fissures, long fine eyelashes with arched brows, malar hypoplasia, myopathic mouth and retrognathia. The child appeared hirsute and was severely delayed, non-verbal and non-ambulatory. Attempts to repair his ptosis have been unsuccessful.

Subject 7 (p.Ile74Asn) was an 8-year-old male, who was referred to clinic at the age of 3 because of psychomotor delay. He is the first child of non-consanguineous healthy parents of Spanish origin. He was born at 38 weeks via an uncomplicated vaginal delivery of a twin pregnancy (bicorial and biamniotic). Birth weight was 2,170 g (<3rd centile). There was no relevant family history. His brother is healthy. Global psychomotor retardation was clear from the first months of life. Clinical examination revealed low growth rate and dysmorphic features (*i.e.*, low hair implantation, downslanting palpebral fissures, hypertelorism, bulbous nose, prominent chin, short neck, short and puffy hands, tapered fingers, separated nipples, and wide thorax). At the age of 5 years, he started with valproic acid for the treatment of generalized seizures. Metabolic studies, karyotype, CGH-arrays and brain MRI were normal. EEG studies demonstrated the presence of generalized spikes and waves during sleep. We conducted a neuropsychological assessment to measure intellectual abilities. Tests revealed a full scale IQ of 53.

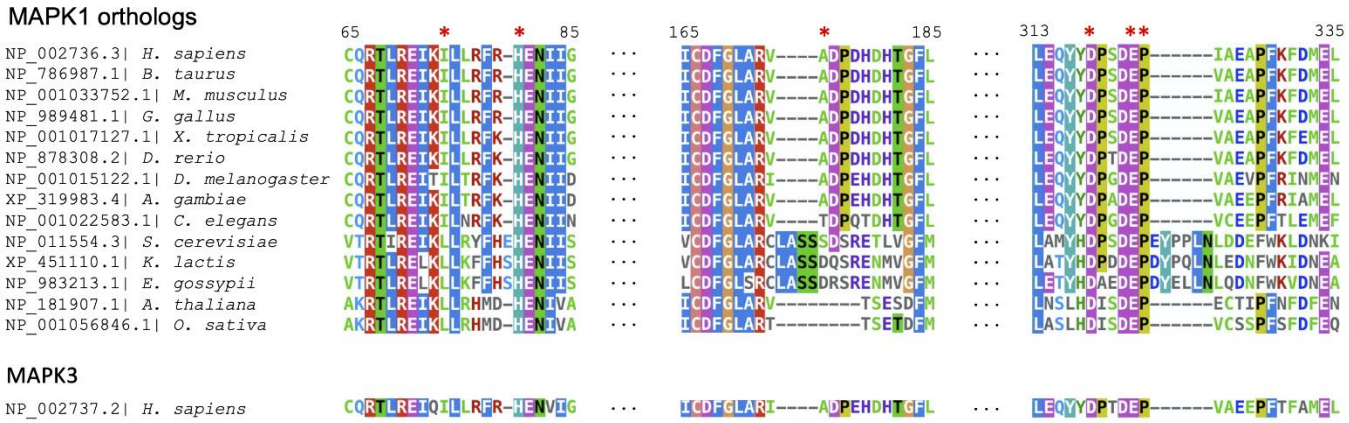

Figure S1. Multiple protein sequence alignment among MAPK1 orthologs and MAPK3.

Protein sequences from MAPK1 orthologs and human MAPK3 (also known as ERK1) were aligned by means of Muscle (v. 3.8) and visualized with MView (v.1.63). Background in consensus positions (identity >70%) is colored according to amino acid biochemical properties. Asterisks indicate the affected residues.

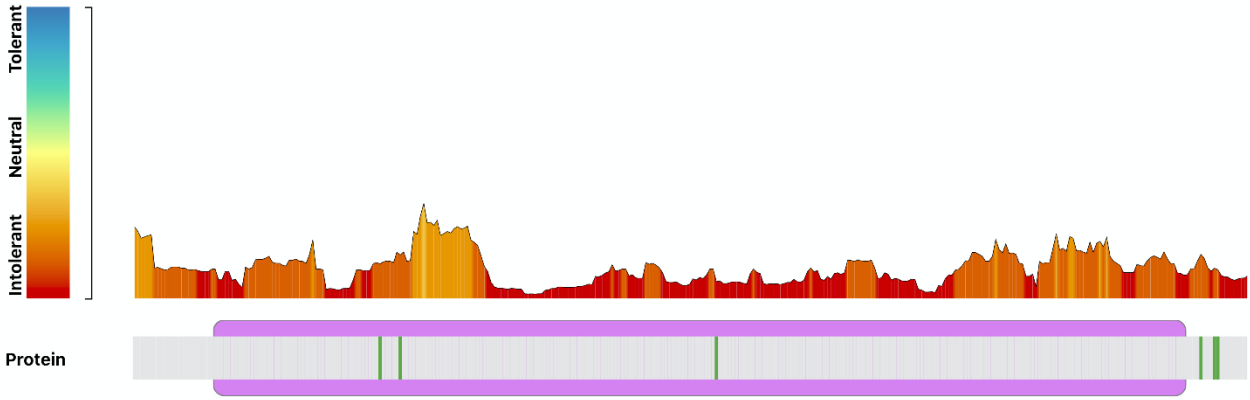

Figure S2. Tolerance landscape of genetic variation for *MAPK1*.

The histograms show the d_N/d_S ratio for individual residues, and are colored according to the scheme reported along the Y-axis. The protein sequence is depicted in grey with the kinase domain (PF00069) shown in violet. The residues affected by the disease-causing mutations identified in the study are shown in green.

Figure S3. The evolving phenotype of Subject 2 with age.

Note: hypertelorism, downslanting palpebral fissures, bilateral ptosis, low-set posteriorly rotated ears, wide nasal bridge, prominent and pointed chin and distal lymphedema (2 years old); bitemporal narrowing, hypertelorism, downslanting palpebral fissures, bilateral ptosis, low-set posteriorly rotated ears, wide nasal bridge, prominent and pointed chin and low posterior hairline (3 years old); in addition to the facial features, note the pectus excavatum, cubitus valgus and bilateral pes planus (7 years old); bitemporal narrowing, hypertelorism, downslanting palpebral fissures, bilateral ptosis (left>right), low-set posteriorly rotated ears, wide nasal bridge, tubular nose, prominent and pointed chin, pectus excavatum, scapular winging, cubitus valgus and bilateral pes planus (11 years old).

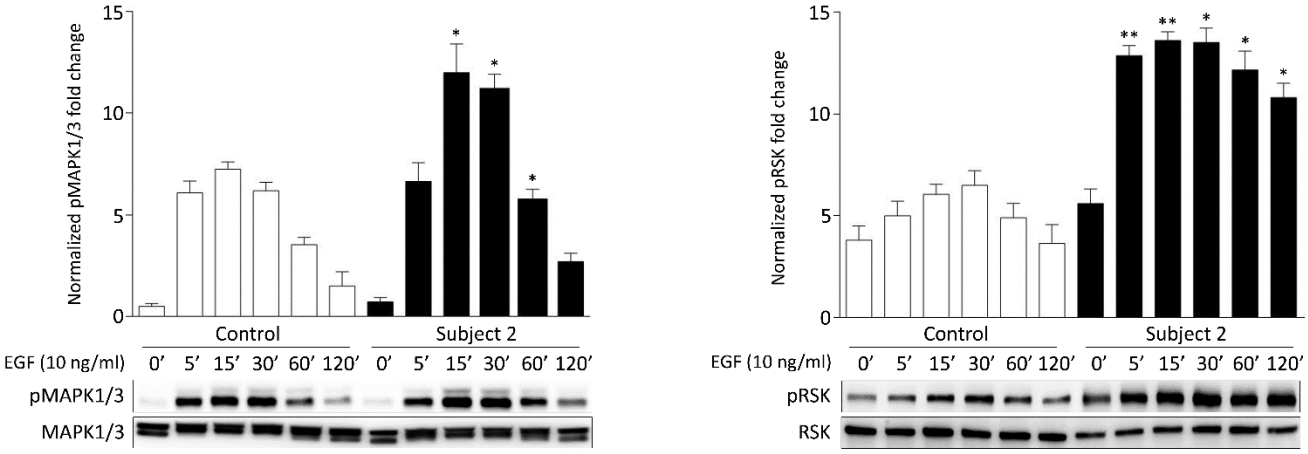

Figure S4. MAPK and RSK phosphorylation assays performed in primary fibroblasts from Subject 2 (p.Asp318Gly).

Representative blots (below) and graphs reporting mean ± SD densitometry values (above) of three independent experiments. Fibroblasts heterozygous for the *MAPK1* variant show higher MAPK1/3 (left) and RSK (right) phosphorylation levels compared to control cells. Cells were starved for 16 h and then stimulated with EGF (10 ng/ml), in time-course experiments, or left unstimulated. Equal amounts of cell lysates were resolved on 10% polyacrylamide gel. Asterisks indicate statistically significant differences in the phosphorylation levels compared to control cells at the corresponding experimental points (* $P<0.05$, ** $P<0.01$; Student's t-test).

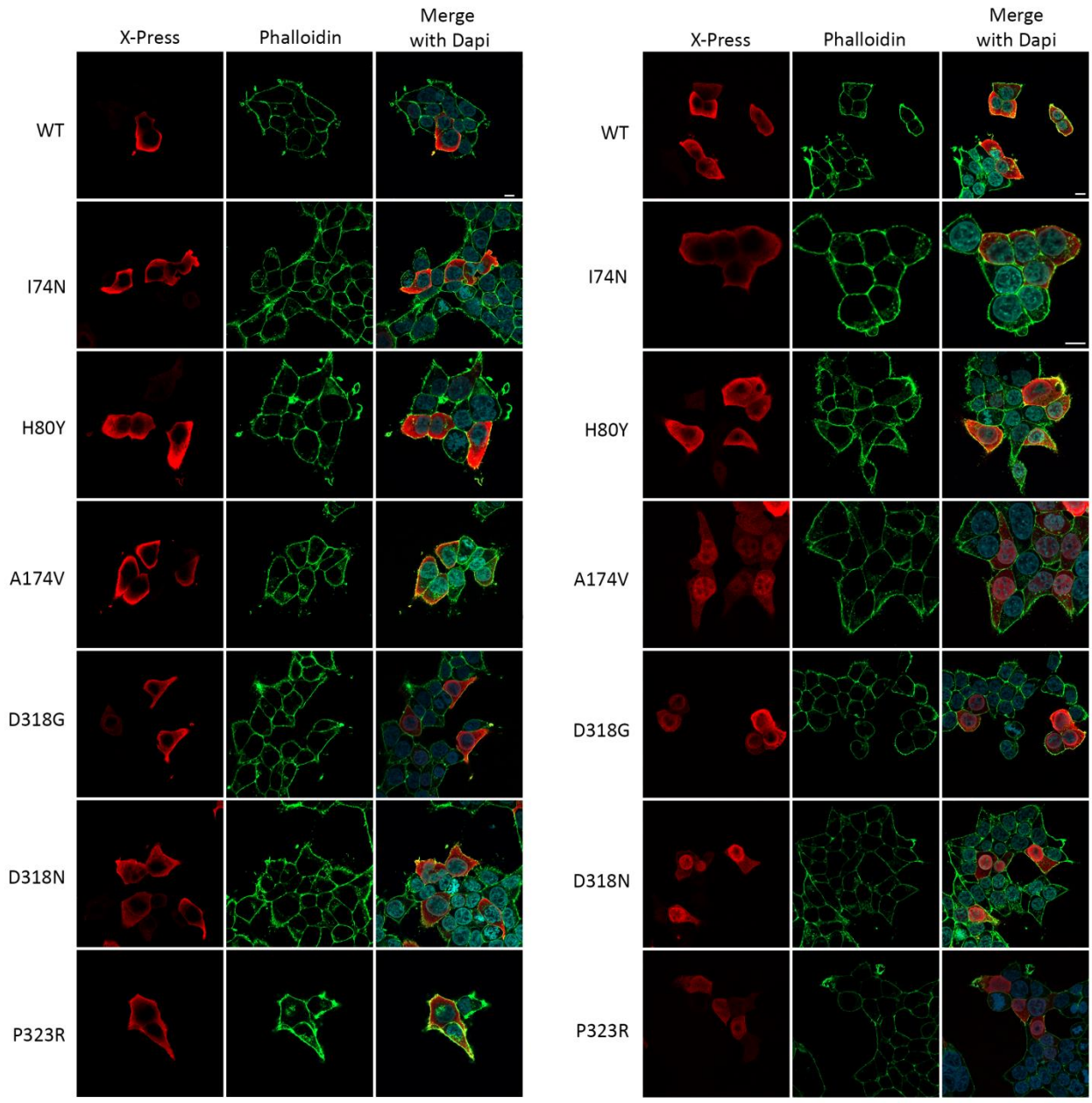

Figure S5. RASopathy-causing MAPK1 proteins show a variably enhanced nuclear translocation in response to EGF stimulation.

MAPK1 subcellular localization showed by confocal laser scanning microscopy observations. Panels represent central sections. Assays were performed in Lenti-X 293T cells transiently expressing Xpress-tagged wild-type and mutant *MAPK1* constructs. Fixed cells were stained with an anti-Xpress mouse monoclonal antibody followed by goat anti-mouse Alexa Fluor-594 (red), and an anti-phalloidin antibody conjugated to green-fluorescent Alexa Fluor 488 dye (green). Nuclei are visualized by DAPI staining (blue). Scale bar is 10 µm.

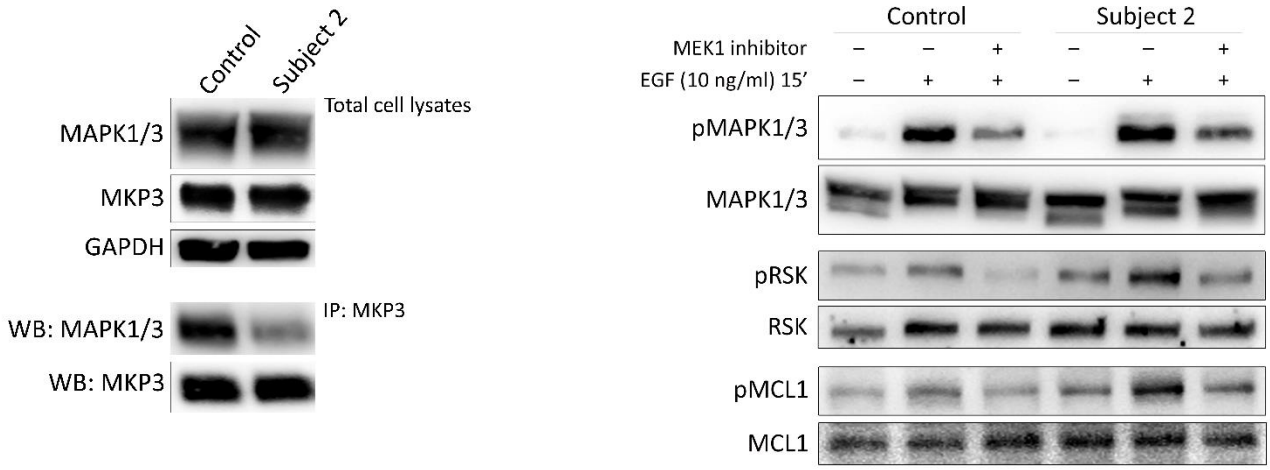

Figure S6. Endogenous MAPK1^{D318G} less efficiently co-immunoprecipitates with MKP3 and retains dependence on MEK activity in upregulating MAPK signaling.

The p.Asp318Gly substitution in MAPK1 impairs proper binding of MAPK1 to MKP3 (left panel). Lysates from primary fibroblasts (Subject 2) were immunoprecipitated with an anti-MKP3 antibody and assayed by western blotting using the indicated antibodies.

MAPK, RSK and MCL1 phosphorylation assays performed in primary fibroblasts (Subject 2) treated with the MEK inhibitor, trametinib (right panel). Assays were performed in cells starved for 16 h and stimulated with EGF (10 ng/ml, 15 min) after treatment with the MEK inhibitor, trametinib (1.5 ng/ml, 2 h). Blots show a comparable decrease in pMAPK, pRSK and pMCL1 in control and patient-derived cells in presence of trametinib, indicating that the mutation-driven signal upregulation of the MAPK cascade retains dependence on MEK activity.

Table S1. WES info and statistics.

ID	WES enrichment kit	Sequencing platform	Target regions covered >10x	Target regions covered >20x	Average depth on target
Subject 1	Agilent SureSelect Clinical Research Exome v2	NextSeq550	95%	91%	98x
Subject 2	Agilent SureSelect V6-All exons	HiSeq X Ten	>99%	98%	153x
Subject 3	Roche SeqCap EZ MedExome	HiSeq 2500	97%	94%	110x
Subject 4	Agilent SureSelect XT Exome v6	NextSeq500	97%	96%	145x
Subject 5	Agilent SureSelect Clinical Research Exome v1	HiSeq 4000	>99%	97%	91x
Subject 6	Agilent SureSelect XT Exome v6	HiSeq 4000	97%	96%	138x
Subject 7	Ion AmpliSeqTM Exome	Ion Proton	91%	83%	84x

Table S2. WES data output.

Subject 1	
Total number of high-quality variants	104,106
Number of variants with predicted functional effect[1]	15,875
Private, clinically associated, and unknown/low frequency variants[2]	268
Putative disease genes (recessive trait)[3]	1[4]
- Filtered candidate genes	none
Putative disease genes (dominant trait)[3]	4[5]
- Filtered candidate genes	*MAPK1*
Subject 2	
Total number of high-quality variants	113,892
Number of variants with predicted functional effect[1]	17,326
Novel, clinically associated, and unknown/low frequency variants[2]	287
Putative disease genes (recessive trait)[3]	none
- Filtered candidate genes[3]	none
Putative disease genes (dominant trait)[3]	4[6]
- Filtered candidate genes	*MAPK1*
Subject 3	
Total number of high-quality variants	86,724
Number of variants with predicted functional effect[1]	27,995
Novel, clinically associated, and unknown/low frequency variants[2]	970
Putative disease genes (recessive trait)[3]	2[7]
- Filtered candidate genes	none
Putative disease genes (dominant trait)[3]	2[8]
- Filtered candidate genes	*MAPK1*
Subject 4	
Total number of high-quality variants	83,499
Novel, clinically associated, and unknown/low frequency variants[2]	1,844
Number of variants with predicted functional effect[1]	707
Putative disease genes (recessive trait)[3]	none
- Filtered candidate genes	none
Putative disease genes (dominant trait)[3]	1[9]
- Filtered candidate genes	*MAPK1*
Subject 5	
Total number of high-quality variants	128,509
Number of variants with predicted functional effect[1]	18,852
Novel, clinically associated, and unknown/low frequency variants[2]	239
Putative disease genes (recessive trait)[3]	none
- Filtered candidate genes	none
Putative disease genes (dominant trait)[3]	2[10]
- Filtered candidate genes	*MAPK1*

Subject 6	
Total number of high-quality variants	357,113
Number of variants with predicted functional effect[1]	39,981
Novel, clinically associated, and unknown/low frequency variants[2]	79
Putative disease genes (recessive trait)[3]	none
- Filtered candidate genes	none
Putative disease genes (autosomal dominant trait)[3]	2[11]
- Filtered candidate genes	*MAPK1*
Subject 7	
Total number of high-quality variants	130.9732
Number of variants with predicted functional effect[1]	52.206
Novel, clinically associated, and unknown/low frequency variants[2]	327
Putative disease genes (recessive trait)[3]	6[12]
- Filtered candidate genes[3]	none
Putative disease genes (autosomal dominant trait)[3]	2[13]
- Filtered candidate genes	*MAPK1*

[1]High-quality non-synonymous SNVs/indels within coding exons and splice regions (-/+8) (subjects 1 and 2); high-quality SNVs/indels within coding exons and splice regions (-/+6) (subject 3); high-quality non-synonymous SNVs/indels within coding exons and splice regions (-/+20) (subject 4); high-quality non-synonymous SNVs/indels within coding exons and splice regions (-13/+6) (subject 5); high-quality non-synonymous SNVs/indels within coding exons and splice regions (-/+30) (subject 6); high-quality non-synonymous SNVs/indels within coding exons and splice regions (-/+5) (subject 7).

[2]High-quality non-synonymous SNV/indels within coding exons and splice regions with gnomAD MAF <0.1% and <1% in public (gnomAD) and in-house (~2,000 population-matched exomes) database (subjects 1 and 2); high-quality SNVs/indels within coding exons and splice regions (-/+6) with MAF <1% ESP6500, dbSNP and in house (~400 exomes, healthy subjects) databases (subject 3); high-quality non-synonymous SNVs/indels within coding exons and splice regions (-/+20) with MAF <1% in public (ExAC) and in-house (860 exomes, healthy subjects) databases (subject 4); high-quality non-synonymous SNVs/indels within coding exons and splice regions with MAF <1% (gnomAD) and <0.1% in-house (~200,000 exomes) databases (subject 5); high-quality non-synonymous SNVs/indels within coding exons and splice regions (-/+10) with MAF <1% in the ExAC database (subject 6); high-quality non-synonymous SNV/indels within coding exons and splice regions with MAF <1% in public (gnomAD) and in-house (~1,200 exomes) databases (subject 7).

[3]Functional impact assessed by Combined Annotation Dependent Depletion (CADD) v.1.4 (http://cadd.gs.washington.edu/), Mendelian Clinically Applicable Pathogenicity (M-CAP) v.1.0 (http://bejerano.stanford.edu/mcap/) and Intervar (http://wintervar.wglab.org) v2.0.1. Variants predicted as benign or likely benign by Intervar were discarded and only those with CADD score >15 or M-CAP score>0.025 were retained (subjects 1, 2 and 5); functional impact assessed using Alamut Visual (Interactive biosoftware) and literature (subject 3); variants were annotated, filtered and prioritized using the Bench NGS Lab platform (Agilent, Leuven, Belgium), functional impact was assessed using Alamut Visual (Interactive biosoftware) and literature (subject 4); functional impact assessed considering 8 predictor systems (SIFT, PROVEAN, MutationTaster, MutationAssessor, LRT, FATHMM, FATHMM-MKL, MetaSVM, MetaLR, GERP,) included in the Varsome engine (https://varsome.com). Private/rare/known

ClinVar pathogenic variants were classified following ACMG criteria (subject 6); functional annotation of the private/rare and HGMD/ClinVar pathogenic variants, was performed by combining 8 predictor systems (SIFT, PolyPhen2, MutationTaster, MutationAssessor, LRT, FATHMM, MetaSVM and CONDEL) included in the ALAMUT (http://www.interactive-biosoftware.com) and ANNOVAR (http://www.openbioinformatics.org/annovar/) packages. Variant categorization was performed following *ACMG* criteria (subject 7).

[4]*DNAH10* (c.1742G>A, p.Arg581Gln; c.13308A>T, p.Arg4436Ser), *TSPYL2* (c.611G>A, p.Ser204Asn, chr X).

[5]*CAPN14* (c.1279-2A>T, splice acceptor variant), *DOC2A* (c.151_152insC, p.Glu51fs), *MAPK1* (c.521C>T, p.Ala174Val), *WIPF2* (c.530_531insGG, p.Pro178fs).

[6]*ADH1B* (c.695G>A, p.Arg232Gln), *HYDIN* (c.11650G>A, p.Glu3884Lys), *KLK12* (c.328C>T, p.Arg110Trp), *MAPK1* (c.953A>G, p.Asp318Gly).

[7]*KLHL10* (c.454T>C, p.Tyr152His; c.887T>C p.Ile296Thr), *ZNF235* (c.424C>G, p.Gln142Glu; c.767T>G, p.Ile256Ser).

[8]*MAPK1* (c.238C>T, p.His80Tyr), *KIAA0368* (c.2407C>T, p.Arg803Trp).

[9]*MAPK1* (c.952G>A, p.Asp318Asn).

[10]*MAPK1* (c.968C>G, p.Pro323Arg), *CACNA1A* (c.6683 G>T, p.Arg2228Leu).

[11]*MAPK1* (c.964G>C, p.Glu322Gln), *MYH3* (c.720C>A, p.Asp240Glu).

[12]*AHNAK2* (c.12374_12376delATG insGCA p.Asp4125_Val4126delinsGlyMet; c.10274C>T, p.Ala3425Val)*, ARHGEF40* (c.1163G>A, p.Arg388Gln; c.2500C>T, p.Arg834Cys), *MAP3K15 (c.806G>A, p.Arg269Gln ;* chr X), *RILPL1* (c.752G>A, p.Arg251Gln, homozygous change), *USP53* (c.1849C>T, p.Pro617Ser; c.2611G>C, p.Gly871Arg), *ZNF81 (c.923T>C, p.Val308Ala,* chr X).

[13]*MAPK1* (c.221T>A, p.Ile74Asn), *WDR48* (c.796C>G, p.His266Asp).

Table S3. Clinical features of subjects with *de novo* pathogenic *MAPK1* variants.

Case ID	Subject 1	Subject 2	Subject 3	Subject 4	Subject 5	Subject 6	Subject 7
Ethnicity	Caucasian	Caucasian	Caucasian	Caucasian	Caucasian	Caucasian	Caucasian
Sex	Male	Male	Male	Female	Male	Male	Male
Age at last examination	13 y 2 mo	12 y	6 y	16 y	3 y 2 mo	15 y	8 y
***MAPK1* variant**							
Genomic position	Chr22(GRCh37): g.22153389G>A	Chr22(GRCh37): g.22127175T>C	Chr22(GRCh37): g.22162017G>A	Chr22(GRCh37): g.22127176C>T	Chr22(GRCh37): g.22123608C>G	Chr22(GRCh37): g.22127164C>G	Chr22(GRCh37): g.22162034 A>T
cDNA change (NM_002745.4)	c.521C>T	c.953A>G	c.238C>T	c.952G>A	c.968C>G	c.964G>C	c.221T>A
Amino acid change	p.Ala174Val	p.Asp318Gly	p.His80Tyr	p.Asp318Asn	p.Pro323Arg	p.Glu322Gln	p.Ile74Asn
Inheritance	*de novo*	*de novo*	*de novo*	*de novo*	*de novo*	*de novo*	*de novo*
gnomAD	not reported	not reported	not reported	not reported	not reported	not reported	not reported
Growth at birth							
Height (SD)	53 cm (+1.65 SD)	47 cm (-2.28 SD)	50 cm (0 SD)	NA	50.8 cm (+0.48 SD)	50.2 cm (+0.17 SD)	47 cm (-1.52 SD)
Weight (SD)	3,650 g (+0.6 SD)	3,350 g (-0.6 SD)	3,672 g (+0.5 SD)	2,610 g (-0.6 SD)	3,657 g (+0.62 SD)	3,062 g (-0.6 SD)	2,170 g (-2.75 SD)
OFC (SD)	NA	33 cm (-1.32 SD)	34.5 cm (+0.66 SD)	NA	NA	NA	33.5 cm (-1.11 SD)
Growth at last examination				16 y (OFC 9y 5mo)		14 y 10 mo	
Height (SD)	157 cm (-0.04 SD)	144.6 cm (-0.82 SD)	105 cm (-2.23 SD)	163 cm (-1.27 SD)	89 cm (-2.21 SD)	122 cm (-5.92 SD)	111 cm (-2.88 SD)
Weight (SD)	45.5 kg (-0.01 SD)	30 kg (-1.99 SD)	17.4 kg (-1.26 SD)	53.5 kg (-0.9 SD)	12.8 kg (-1.13 SD)	16.1 kg (-7.77 SD)	18 kg (-2.65 SD)
OFC (SD)	59 cm (+2.82 SD)	52 cm (-1.01 SD)	48.5 cm (-2.39 SD)	54 cm (+0.47 SD)	48.5 cm (-1.34 SD)	44 cm (-7.4 SD)	48 cm (-3.25 SD)
Development							
DD	yes	yes	yes	yes	yes	yes	yes
ID	no	yes	yes	yes	yes	yes	yes
Language delay	no	yes	yes	yes	yes (speech apraxia)	yes	yes
Behavioral problems	anxiety and reduced stress tolerance	ADHD	aggressive, destructive, spitting, head banging	ADHD	very active, destructive, affectionate, ASD	occasionally aggressive	severe ADHD
Learning disorder	yes	yes	yes	yes	yes	yes	yes

Case ID	Subject 1	Subject 2	Subject 3	Subject 4	Subject 5	Subject 6	Subject 7
Neurological							
Hypotonia	no	yes	yes	no	no	yes (axial hypotone with increased distal tone)	yes
Epilepsy	no	no	no	no	yes (4mo, infantile spasms, controlled with vigabatrin)	no	yes (5y, generalized seizures, controlled with valproic acid)
CHD	mitral regurgitation, mitral valve prolapse, patent foramen ovale	ASD and mild mitral valve prolapse	no	mitral valve billowing	ASD	no	no
Skeletal anomalies	pes planus, scapular winging, cubitus valgus	pes planus, mild legs asymmetry (5 mm)	broad thorax, pes planus	broad thorax	tapered fingers, with broad bast at MP joints tapering to the distal phalanges, scapular winging	dextroconvex thoracolumbar scoliosis, dislocation/subluxation of the left femoral head, clinodactyly, overlapping toes, prominent heels, bilateral clubfoot, limited elbow extension	hyperlaxity, short and puffy hands and feet, tapered fingers, mild metatarsus varus
Facies	epicanthal folds, blue eyes, hypertelorism, low-set posteriorly rotated ears, webbed/short neck	prominent metopic ridge, bitemporal narrowing, hypertelorism, downslanting palpebral fissures, ptosis, low-set posteriorly rotated ears, wide nasal bridge, prominent and pointed chin, low posterior hairline	high forehead, medial thin and flaring of eyebrows, ptosis, slightly wide nasal bridge when younger, round nasal tip (upturned), posteriorly rotated ears, small teeth, fusion of two teeth, webbed/short neck	broad forehead, full eyebrows, hypertelorism, ptosis, short and almond-shaped palpebral fissures, posteriorly rotated ears, full lips, hypertrichosis, hoarse voice, low posterior hairline	hypertelorism, ptosis, wide mouth, full lips, small lower incisors, widely spaced teeth, webbed/short neck	microcephaly, plagiocephaly, highly arched eyebrow, long eyelashes, downslanted palpebral fissures, severe ptosis (unsuccessfully treated), malar hypoplasia, low-set posteriorly rotated ears, carp-shaped mouth, long philtrum, crowded teeth, mandibular micrognathia, coarse facies, generalized hirsutism, low posterior hairline	prominent metopic ridge, bitemporal narrowing, mild hypertelorism, downslanted palpebral fissures, ptosis, low-set posteriorly rotated ears, wide nasal bridge, high arched palate, widely spaced teeth, pointed chin, low posterior hairline, webbed/short neck

Case ID	Subject 1	Subject 2	Subject 3	Subject 4	Subject 5	Subject 6	Subject 7
Other features							
Skin and annexes	curly and thick hair, multiple lentigines	1 *cafè au lait* spot, 3 hypochromic spots	dry skin, mild eczema	hypertrichosis	dry skin	freckling (forehead), several 5-10 mm hyperpigmented macules (feet, dorsal), thin nails, hypertrichosis	no
Cryptorchidism	no	yes	no	no	no	yes	no
GER	no	no	wet lung syndrome	no	history of aspiration	yes	no
Recurrent Infections	no	no	yes (ears)	yes (ears)	no	no	no
Lymphatic involvement	no	periphery lymphedema	no	no	no	no	no
Bleeding/easy bruising	no	no	yes	no	no	no	no
Auditory issues	no	no	no	no	no	no	no
Others features				Tietze syndrome			
Imaging and laboratory findings							
MRI/CT	not performed	cavum setto pellucido	mild widening frontal peripheral liquor spaces (1 mo)	not performed	normal (4 mo)	not available	normal
Abdominal U/S	not performed	normal	normal	not performed	duplicated collecting system of the right kidney	suspicious for bowel malrotation, inflammatory bowel disease (Crohn's disease), marked atrophy of the left kidney	no

ADHD, attention deficit hyperactivity disorder; ASD (behavioral problems), autistic spectrum disorder; ASD (CHD), atrial septal defects; CHD, congenital heart defects; DD, developmental delay; ID, intellectual disability; OFC, occipitofrontal circumference.

Table S4. Vulval phenotypes in *mpk-1*(*pan14*[D321G]) knock-in *C. elegans* hermaphrodites and in worms overexpressing a subset of disease-causing *MAPK1* mutant alleles under the control of p*lin-31*.

Genotype	**Transgene**	**Multivulva (Muv) phenotype (%)**	**Vulvaless (Vul) phenotype (%)**	***N***
WT	-	0	0	>1,000
mpk-1(*pan14*[D321G])	-	0.5	0	1,000
WT	empty vector	0	0	231
WT	*MAPK1*^{WT}	0	0	639
WT	*MAPK1*^{I74N}	0.4	0	441
WT	*MAPK1*^{H80Y}	1.0[a]	0	479
WT	*MAPK1*^{A174V}	1.2[b]	0	651
WT	*MAPK1*^{D318G}	1.4[b]	0	370
WT	*MAPK1*^{P323R}	2.0[c]	0	492
let-23(sy1)	-	0	85.0	939
let-23(sy1); mpk-1(*pan14*[D321G])	-	0.9[d]	58.9[e] [*r*=30.7]	555
let-23(sy1)	*MAPK1*^{WT}	0	79.8[f] [*r*=6.1]	297
let-23(sy1)	*MAPK1*^{I74N}	0	78.0 [*r*=9.2]	295
let-23(sy1)	*MAPK1*^{H80Y}	0.7	70.7[g] [*r*=16.8]	300
let-23(sy1)	*MAPK1*^{A174V}	0.5	76.9 [*r*=9.5]	221
let-23(sy1)	*MAPK1*^{D318G}	1.1[d]	63.1[h] [*r*=25.8]	253
let-23(sy1)	*MAPK1*^{P323R}	0.7[d]	69.8[i] [*r*=17.9]	567

The c.962A>G variant leading to the p.Asp321Gly amino acid substitution, corresponding to the human p.Asp318Gly change, was introduced in the *C. elegans mpk-1* gene by CRISPR-Cas9. As a complementary approach, wild-type (WT) *MAPK1* and five disease-causing mutants were overexpressed under the control of the *lin-31* promoter, which drives expression principally in vulval precursor cells.

Multivulva (Muv) and vulvaless (Vul) phenotypes are expressed as percentage of adult animals displaying multiple ectopic pseudovulvae or lacking a vulva, respectively.

let-23(sy1) is a hypomorphic allele of *let-23*, homolog of the human gene encoding the EGF receptor. *N* indicates the number of animals scored; *r* specifies the rescue of the Vul phenotype associated with homozygosity for the *let-23*(*sy1*) allele expressed as percentage (|[%Vul/85-1]|x100). A single letter code is used to specify amino acid changes.

In all comparisons, *p* values were calculated using two-tailed Fisher's exact test.
[a-c] Significantly different from animals expressing *MAPK1*^{WT} ([a] $p < 0.02$; [b] $p < 0.01$; [c] $p < 0.0005$).
[d-f] Significantly different from *let-23(sy1)* animals ([d] $p < 0.02$; [e] $p < 0.00001$; [f] $p < 0.05$).
[g-i] Significantly different from *let-23(sy1*) animals expressing *MAPK1*^{WT} ([g] $p < 0.02$; [h] $p < 0.00002$; [i] $p < 0.002$).